



## Supplementary Materials for

### **A single gene orchestrates androgen variation underlying male mating morphs in ruffs**

Jasmine L. Loveland *et al.*

Corresponding authors: Jasmine L. Loveland, [jasmine.loveland@univie.ac.at](mailto:jasmine.loveland@univie.ac.at); Alex Zemella, [alex.zemella@bi.mpg.de](mailto:alex.zemella@bi.mpg.de); Clemens Küpper, [clemens.kuepper@bi.mpg.de](mailto:clemens.kuepper@bi.mpg.de)

*Science* **387**, 406 (2025)  
DOI: 10.1126/science.adp5936

#### **The PDF file includes:**

Materials and Methods  
Figs. S1 to S11  
Tables S1 to S8  
References

#### **Other Supplementary Material for this manuscript includes the following:**

MDAR Reproducibility Checklist

## **Materials and Methods**

### **Animal breeding**

We collected 36 male ruffs from a captive research flock held in outdoor pens at Simon Fraser University mornings between the 5<sup>th</sup> and 17<sup>th</sup> of June in 2017, 2018, and 2019 (24, 25, 56). Each male was observed multiple times during the days prior to sample collection to ensure that they expressed morph-specific social behaviors such as aggressive defense of small courts (independents), courtship (satellites and independents) and affinity to females (all three morphs). We kept focal males in mixed-morph male pens with a view through netting partition of an adjacent pen holding 20-30 females. The captive flock were held under Canadian Wildlife Service permits; housing and collection procedures were approved by the Animal Care Committee of Simon Fraser University (permit #1232B-17) operating under guidelines from the Canadian Council on Animal Care.

### **Sample allocation**

Tissue samples from 36 birds (17 independent, 10 satellite and 9 faeders) were allotted as follows. Testes and blood for hormone measurements and organs were collected for all 36 birds and samples for RNA-Seq were processed as shown in table S4. Of these, brains processed for RNA-Seq included 19 birds (9 independents, 5 satellites and 5 faeders), data from one independent male was dropped due to poor RNA quality. We processed blood for RNA-Seq for nine birds (three per morph). Testosterone and androstenedione were measured in single testes of 36 birds. Testosterone was measured from plasma in 36 birds and androstenedione was measured in plasma and testes of 25 and 36 birds, respectively.

### **Behavior scoring**

To compare social behaviors between morphs we filmed 27 focal birds (9 independents, 9 satellites, 9 faeders) to obtain at least 5 min of scorable behaviors (video time length scored: mean  $\pm$  SEM = 7.09  $\pm$  0.65 min). Behavior for one satellite bird was lost because the file was corrupted, resulting in final sample sizes of 9 independents, 8 satellites, 9 faeders. We calculated frequency of each behavior based on the total time that each bird was scored. We scored a total of 14 behaviors (table S5) performed by focal males and used nine behaviors for the analysis of aggression (chase, peck, forward, fight) and courtship (full squat, mutual squat, circle, half-circle, mount) across morphs using BORIS (version 7.9 - 2019-10-24); these results were published previously in (38). Scoring was done by an experimenter blind to the experimental design and ID. We used previous descriptions of ruff male behavior (23, 57, 58) with minor modifications listed in table S5. We counted the number of times each behavior occurred and the duration of each behavior except for 'peck', which was only scored as an event. We noted the occurrence and duration of when the focal bird was out of view from the camera as an 'out of screen' event, therefore the total time each bird was scored was variable. We also scored an additional 6 events: whether the focal male crouched (appearing to be receptive to mounting; this posture is usually only seen in faeder males), strutted (a walk with full body erect, chest out, resembling a 'tip-toe' walk), was mounted by another male, was circled or half-circled by another male, or was chased by another male, resulting in a total of 21 scorable events.

### **Tissue and blood collection, brain area dissections overview and RNA extraction**

We collected brains, pituitaries, adrenals, livers and testes for each of the three ruff mating morphs (17 independent, 10 satellite and 9 faeders), for a total of 229 adult samples (table S4). All

birds were killed by rapid decapitation. After decapitation we collected blood from the decapitation site and placed it on ice, extracted the brain, weighed it and froze it immediately in a plastic mold filled with embedding medium (Neg 50, Thermo Scientific) on dry ice and then immediately continued to collect pituitary, liver, adrenals and one testis into RNALater following manufacturer's instructions. We placed the alternate testis on dry ice in either embedding medium or in aluminum foil. We centrifuged blood at 2500g for 15 min and collected the plasma for hormone measurements. All samples were stored at  $-80^{\circ}\text{C}$  until shipping to Germany on dry ice within 1-2 months from date of collection and then stored again at  $-80^{\circ}\text{C}$  until further processing.

We sectioned thick coronal slices of brains (200  $\mu\text{m}$ ) on a cryostat (Leica). We allowed slices to thaw briefly to adhere to slides (Superfrost), photographed the entire slide to use as reference during microdissections, and placed the slide in a box which was temporarily stored on dry ice and then at  $-80^{\circ}\text{C}$ . To microdissect brain areas we thawed each slide by brief submersion in ethanol (30 s), then phosphate buffered saline (PBS) (5 s) followed by immediate collection of brain areas of interest under a dissection microscope (fig. S1). Further details are given in the section 'Sampling of brain regions'. We placed the microdissected brain areas in tubes filled with 400  $\mu\text{l}$  of lysis buffer (RLT buffer from RNeasy Mini Kit supplemented with beta-mercaptoethanol) kept on dry ice and then stored at  $-80^{\circ}\text{C}$  until RNA extractions.

We extracted total RNA from microdissected brain areas and organ samples using the RNeasy Mini Kit (Qiagen) according to manufacturer's instructions. One modification was that we homogenized testicular tissue and filtered it through QIAshredder columns before initiating the RNA isolation protocol. We quantified RNA concentration and RNA to protein ratios (A260/A280) on a NanoDrop 2000 spectrophotometer (Thermo Fisher Scientific). We measured RNA integrity numbers (RINs) with RNA Nano Chips on an Agilent 2100 Bioanalyzer (Agilent Technologies). We diluted RNA samples and re-measured concentrations with the Qubit RNA BR Assay Kit (Thermo Fisher Scientific) on a Qubit Fluorometer.

### Sampling of brain regions

Currently there is no brain atlas for the ruff or any other shorebird species. Therefore, we used previously published atlases and studies from chicken (59, 60), quail (61, 62), crow (63) and the revised nomenclature for avian brain nuclei (64) to aid in identifying regions of interest in the ruff brain. First, we identified brain nuclei by analyzing the distribution of cells and cytoarchitecture in eight independent male ruff brains that were sectioned 40  $\mu\text{m}$  thick and Nissl-stained (65) and one female brain that was stained for immunohistochemical detection of serotonin following the protocol described in ref. (66). Next, we microdissected brain nuclei as described below while also using the pictures of slides containing sections for RNA-Seq as a guide.

All descriptions are given from 'start' to 'end' of collection going in the anterior to posterior direction. Due to variability in the angle of sectioning, sometimes collection of left and right sides ended on different sections because we adhered to using specific landmark criteria to decide where to best limit collection (fig. S1). We collected nodes within the social behavior network (28) as follows. For the lateral septum (LS) collection began where the lateral ventricle was clearly visible and ended once the anterior commissure crossed the midline. For the arcopallium and nucleus taenia (A+TnA) collection began where the tractus septopallio-mesencephalicus (TSM) changed from straight to curved and ended on the first section where part of the optic tectum first appeared. Medial preoptic area (POM) collection began where the TSM along the midline changed from straight to curved and ended one section after the anterior commissure crossed the midline. This ensured that we collected the POM in the majority of its antero-posterior extent, such that it would

certainly contain the anterior and medial preoptic area (AMPO and MPO according to ref. (59)). It is possible that with this method we also collected a portion of the anterior hypothalamus as defined by ref. (60) and the periventricular hypothalamic nucleus (PHN, (67), which is not the same as the hypothalamic periventricular organ, see below). However, our methodology in collecting the POM ensured i) a reduction of variability that may have been introduced by the angle of sectioning and ii) that all POM samples were nearest to the anterior commissure. Therefore, our POM samples correspond to the areas that are labeled as the median preoptic nucleus (MnPO) and medial preoptic nucleus (MPO) in chicken (59); the posterior most part of the nucleus preopticus periventricularis (POP) and the nucleus periventricularis hypothalamic (PHN) in chicken (67); the POM under the anterior commissure in (68, 69); and the POM-1 area (also called POMn, nucleus preopticus medianus) in quail as described in (70). For the hypothalamus (HYP), collection started immediately after the last section where POM was collected from and ended on the anterior most section preceding the first section where VTA+SN were collected. Hypothalamus samples therefore included most or all of paraventricular and anterior hypothalamic nuclei; ventromedial, lateral and posterior hypothalamic nuclei in their entirety; hypothalamic periventricular organ (HPO) and the distal cell group of the HPO, the HPD, in their entirety; and partial or all arcuate nucleus (nomenclature as per ref. (59)). The caudal nidopallium (NC) is not part of the social behavior network and does not have clear markers for its borders in fresh tissue. Therefore, we collected only a small lateral portion of the NC, dorsal from the arcopallium on the posterior most sections, where we had collected A+TnA from.

We collected the ventral tegmental area and substantia nigra (VTA+SN) as part of the mesolimbic reward system (29, 71), which contain populations of dopaminergic neurons and the raphe (RAP), which contains the largest and most dense cluster of serotonin-producing neurons that project throughout the entire brain (72). For the VTA+SN, collection started one section before the oculomotor cranial nerve (NIII) appeared and one section after NIII was no longer visible, to ensure the majority of sections contained the full extent of the NIII, a well-known marker for the location of A9 and A10 dopaminergic neuron populations (73). For the raphe (RAP), collection began immediately after the last section collected for VTA+SN. We made the shape of the dissected area in the form of an inverted triangle so that the top part could prevent us missing possible serotonin cells around the medial longitudinal fasciculus. The inverted triangle shape also allowed us to capture the parallel sheets of serotonin cells that typically populate the midline (63).

For six of the seven brain areas we targeted, we confirmed post-hoc the accuracy of dissection by examining expression of specific molecular markers. We found highest expression of the following genes in expected brain areas, compared to the rest of the brain, as follows: *TPH2*, the rate-limiting enzyme for serotonin synthesis, and *HTR1A*, in the raphe; *TH*, the rate-limiting enzyme for dopamine synthesis in the VTA+SN; *CIQL3* and *ETV1* in the A+TnA (74); *OXTR*, which has been shown to have well-defined and abundant expression by *in situ* hybridization in the septum of other bird species (75), in the LS; putative vasotocin-neurophysin (*LOC106902922*), oxytocin (*LOC106902860*) and aromatase (*LOC106889446*) in the POM and HYP; *PENK* and *GAL* in the POM. To check dissection accuracy of pituitary samples, we also confirmed high expression of genes encoding anterior pituitary hormones (fig. S9).

#### Blood processing for RNA-Seq

At time of blood collection, we mixed 200 µl of blood with 750 µl of TRI Reagent BD (Sigma) followed by vigorous shaking. We then placed the tube on ice and stored it on dry ice and then at -80 °C until further processing. We thawed samples and added 20 µl of 5N acetic acid to

each sample and mixed. We then passed samples through a QIAshredder column (Qiagen), centrifuged at 12000g for 3 min at room temperature and repeated this step with the eluate. We transferred the eluate to a new tube and added 200 µl of chloroform, vortexed and let sit at room temperature for 2-3 min before centrifuging at 12000g for 18 min at 4 °C. We transferred the clear supernatant to a new tube and mixed with 1 volume of 70 % ethanol by pipette. We passed half of the mixture through a miniprep column (RNeasy Mini Kit, Qiagen) with centrifugation at 8000g for 20 s, and then repeated again on the same column with the second half, and discarded the eluates. We proceeded with the RNA extraction protocol as per the manufacturer's instructions. We eluted RNA in 30 µl of RNase-free water, placed the RNA on ice and froze at -80 °C until further processing.

### Bulk RNA-Seq library preparation

Prior to sequencing, we assessed total RNA quality using a Fragment Analyzer 5200 (Agilent). Polyadenylated RNA enrichment was performed using the NEBNext Poly (A) mRNA Magnetic Isolation Module Kit (New England BioLabs). RNA libraries were synthesized using the NEBNext Ultra II Directional RNA Library Preparation Kit for Illumina (New England Biolabs). 250 ng of total RNA from each sample was subjected to 100 bp paired-end sequencing on an Illumina NovaSeq 6000 (12 PCR cycles) according to Illumina protocols. Conversion of binary base call (BCL) sequence files and demultiplexing were performed using bcl2fastq2 v2.2.0. Library preparation and sequencing were executed by the DRESDEN-concept Genome Center.

### RNA-Seq data processing and variant discovery

Adapters and low-quality bases (<Q30) were removed using TrimGalore version 0.6.7 (<https://github.com/FelixKrueger/TrimGalore>) with the parameters '--illumina -q 30 --length 50'. We aligned the trimmed RNA reads to the *Calidris pugnax* reference genome [[GCF\\_001431845.1](https://www.ncbi.nlm.nih.gov/assembly/GCF_001431845.1)] using STAR version 2.7.10a (76) with the RefSeq annotation gtf file. Morph-specific variants within the autosomal inversion regions were identified following GATK's best practices (GATK version 4.2.6.1) framework (77). We assigned all RNA reads in each library to a new read-group name using Picard-AddOrReplaceReadGroups, and then removed sequencing duplicate reads using Picard-MarkDuplicates. RNA reads were sorted by coordinates using Picard-SortSam and reads containing Ns in their cigar string were split into new reads using GATK-SplitNCigarReads. We identified variants by running the GATK genomic variant call format (GVCF) workflow. First, we used GATK-HaplotypeCaller with the flag '-ERC GVCF' to generate GVCF files for each sample with all sites within the autosomal inversion regions which is located on scaffold 28 in the reference assembly. Next, we used GATK-CombineGVCFs to combine all the GVCF files into a multi-sample single GVCF file. We used GATK-GenotypeGVCFs to perform joint genotyping on all samples in the final VCF file to call the variable sites only. We retrieved biallelic single nucleotide polymorphisms (SNPs) and insertions/deletions (InDels) for each ruff morph and filtered them separately using GATK recommended parameters for hard-filtering germline short variants (<https://gatk.broadinstitute.org/hc/en-us/articles/360035890471-Hard-filtering-germline-short-variants>). For faeder and satellite samples, we manually converted calls of homozygous variants of inversion alleles into heterozygous variants because the two morphs are obligate heterozygotes for the inversion regions (20). Since our goal was to examine allelic differences between ancestral independents and derived satellites and faeders, we removed variants that were shared between independents and any of the other two morphs using bcftools version 1.18 (78). This resulted in two VCF files of consensus biallelic heterozygous SNPs and InDels within the

autosomal inversion regions for both satellite and faeder morphs, respectively, which we used for subsequent analyses. All identified variants were further annotated to examine functional consequences using Ensembl VEP (Variant Effect Predictor) tool version 110 (79) with the parameter ‘--everything’.

#### Allele-specific expression analysis

The *Calidris pugnax* reference genome was generated using an independent male (26). To account for mapping bias towards the independent allele of inversion genes in satellites and faeders, we used the STARconsensus method (80) in STAR version 2.7.10a. Briefly, the previously generated biallelic heterozygous SNPs and InDels vcf files were incorporated to the reference genome to generate consensus genomes for the satellite and faeder morphs, separately, each containing morph-specific inversion haplotypes. Then, we aligned faeder and satellite RNA-Seq reads to the corresponding genomes using STAR in multi-sample 2-pass mode, after collecting splice junctions from all the samples. We measured allele-specific expression following suggested best practices (81). First, we removed sequencing duplicates from the aligned RNA-Seq reads using GATK-MarkDuplicates. We then performed allele counting at each heterozygous site for all genes within the boundaries of the autosomal inversion using GATK-ASEReadCounter. The minimum mapping quality and minimum base quality were set to 50 and 25, respectively. Raw allele counts for each sample were normalized by library size, and filtered to keep only exonic variants. Significant allele-specific expression sites were determined by two-tailed binomial tests with Benjamini-Hochberg correction for multiple testing ( $FDR < 0.05$ ). We separated significant allele-specific expression into overexpression and underexpression of the inversion allele by dividing the inversion allele count by the total read count. An inversion allele proportion of  $>0.5$  indicates overexpression (up-regulation of the inversion allele) and  $<0.5$  indicates underexpression (down-regulation of the inversion allele), relative to the non-inverted allele.

#### Differential gene expression analysis

For each tissue we constructed a gene count matrix by combining gene counts from the independent samples following alignment to the ruff reference genome accessed through National Center for Biotechnology Information (NCBI) RefSeq: GCF\_001431845.1, and gene counts for the satellite and faeder samples following alignment to their respective STAR-consensus genomes. Normalization and differential gene expression analysis between ruff morphs was performed using DESeq2 version 1.42.0 (82). We included known batch effects into the model and filtered out low-abundance genes below a mean count of five reads across the smallest morph sample size. In our analyses, we examined data at two levels of resolution, tissue and morph. At the tissue level, we conducted separate analyses for each brain area and body tissue, employing the design model ‘~Batch+Morph’, resulting in a total of 33 comparisons. At the morph level, we included all 229 samples in the input count matrix data and applied the design model ‘~Batch+Tissue+Morph’, for a total of three comparisons. We computed the differential gene expression analyses by setting the reference level for the Morph covariate to independent for the faeder vs. independent and satellite vs. independent comparisons and to satellite for the faeder vs. satellite comparisons, respectively, before running DESeq2. Then, the ashR method was used for log<sub>2</sub>-transformed FC value correction. We considered genes as differentially expressed when their adjusted p-values from DESeq2 were lower than  $<0.05$  after Benjamini-Hochberg correction.

We performed principal component analysis (PCA) based on the top 1000 genes with the greatest variance in gene expression using ‘plotPCA’ in DESeq2 after transforming the normalized

count data with the ‘varianceStabilizingTransformation’ function. We modified misannotated or non-descriptive gene symbols as follows: Prior to running DESeq2, we reassigned gene symbols for a subset of genes that were misannotated as paralogs in the ruff reference [RefSeq: GCF\_001431845.1]. For non-descriptive ‘LOC’ names, we use the predicted ortholog gene name with the suffix ‘-like’ in Figures. A list of these gene symbol modifications for the inversion region is provided in table S6. A full list of gene symbols and descriptions for genes shown in main and supplementary Figures is given in table S7.

### Functional enrichment analysis

As the current *Calidris pugnax* assembly lacks a functional annotation of the genes, we used eggNOG-mapper version 2.0.9 (83) for the annotation of protein sequences. We used the function ‘makeOrgPackage’ from the R package AnnotationForge version 1.44.0 (84) to create a custom *Calidris pugnax* organism database with up-to-date gene annotations for this species. We tested lists of differentially expressed genes obtained from DESeq2 for functional enrichment of GO terms using the function ‘enrichGO’ in clusterProfiler version 4.10.0 (85). Up- and down-regulated genes were analyzed separately using appropriate genome background gene lists for each tissue. To account for multiple testing, we used a Q-value <0.1 as threshold for statistical significance.

### Validation of gene expression results through quantitative PCR (qPCR)

We used qPCR results from RNA extractions for five genes in a limited set of tissues (pituitary: *PGR*, *FSHB*, *GNRHR3*; testes: *STAR* and *HSD17B2*) belonging to 33 of the 36 birds to validate the RNA-Seq data used in the present study (fig. S10). The qPCR results from the same RNA extraction for 25 genes had been published previously (24, 25).

### Plasma androgen measurements

Data reported in Figures 1B, S8 and table S3 for circulating testosterone and androstenedione were measured and reported previously in refs (24, 25).

### Measurement of testicular androgens

At time of collection, we weighed each testis and calculated the weight of paired testes (mean = 3.1 g, range 1.9 – 4.4 g). After storage at -80 °C, a single testis that had been frozen in foil or embedding media was thawed and a portion was cut and weighed (mean = 138 mg, range 55 – 215 mg) and frozen again until further processing. At the start of the hormonal extraction, dissected testes pieces were thawed again and placed each in a glass vial on ice and then sonicated with 1 ml of ddH<sub>2</sub>O. Next, each sample was vortexed and fractions (200 µl) transferred to two new glass vials, to which either 1500 dpm 3H-testosterone or 3H-androstenedione (Perkin Elmer, Rodgau, Germany) was added to determine extraction efficiency. After vortexing, samples were incubated over night at 4 °C. Then, hormones were extracted using 4 ml of a 30 % / 70 % petroleum ether / diethyl ether mixture, by snap-freezing the lower water phase and decanting the ether phase (repeated twice). The ether phase was dried at 37 °C under a stream of nitrogen and 1 ml ethanol (100 %) added over night to precipitate proteins at -25 °C. After adding 100 µl of ddH<sub>2</sub>O samples were washed twice with 2 ml of hexane. After drying under a stream of nitrogen, samples were resuspended in phosphate buffered saline with 1 % gelatin (PBSG). An aliquot was transferred to scintillation vials, mixed with 4 ml scintillation fluid (Packard Ultima Gold) and counted to an accuracy of 2-3 % in a Beckman LS 6000 β-counter to estimate extraction efficiency, which was 77.8 ± 6.1 % for testosterone and 66.9 ± 3.0 % for androstenedione.

Testosterone and androstenedione contents were determined by radioimmunoassay following previously published protocol (86). Briefly, a standard curve was set up in duplicates by serial dilution of stock standard testosterone and androstenedione ranging from 0.39 – 200 pg. Testosterone and androstenedione antisera (Esoterix Endocrinology, Calabasas, CA, USA) were added to the respective standard curve, the controls and to duplicates of each sample (100 µl). After 30 min the respective testosterone or androstenedione label was added and the assays incubated for 20 hours at 4 °C. Then, bound and free fractions were separated at 4 °C by adding 0.5 ml dextran-coated charcoal in PBSG assay buffer. After 14 min incubation with charcoal, samples were spun (3600g, 10 min, 4 °C) and supernatants decanted into scintillation vials at 4 °C. After adding 4 ml scintillation liquid (Packard Ultima Gold) vials were counted. Standard curves and sample concentrations were calculated with Immunofit 3.0 (Beckman Inc. Fullerton, CA), using a four-parameter-logistic-curve fit. Data were analyzed in one assay for testosterone and androstenedione, respectively. The lower detection limits of the standard curves were determined as the first value outside the 95 % confidence intervals for the zero standard ( $B_{max}$ ) and were 3.0 pg/ml for testosterone and 7.3 pg/ml for androstenedione. The intra-assay coefficient of variation as determined by extracted chicken plasma pools was 3.8 % for testosterone and 6.8 % for androstenedione. Because the testosterone antibody used shows significant cross-reactions (44 % according to the specification sheet provided by the manufacturer) with 5-alpha-dihydrotestosterone our testosterone measurement may include a fraction of 5-alpha-dihydrotestosterone.

#### Ruff HSD17B2 homology model

The HSD17B2 protein currently has no available crystallographic structure and a manually curated homology model is only available for human HSD17B2 (41). Hence, we conducted in silico homology modelling for HSD17B2 homodimers using the protein sequences of each of the three ruff alleles. First, we used the independent (ancestral) HSD17B2 protein sequence (XP\_014797711.1) truncated to contain only residues 86 to 376, as query in AlphaFold2-Multimer (ColabFold v1.5.5) with default settings. AlphaFold2 allows to make predictions of three-dimensional protein structures with atomic-level accuracy (87). We then generated the satellite and faeder HSD17B2 structures by manually introducing the corresponding mutant residues to the independent HSD17B2 structure with the ‘mutagenesis’ tool in PyMOL (The PyMOL Molecular Graphics System, version 2.0 Schrödinger, LLC.) (Fig. 3D).

#### Molecular docking predictions and binding affinity measurement

We obtained canonical testosterone and nicotinamide adenine dinucleotide ( $NAD^+$ ) files in structure-data format (SDF) (testosterone 6013;  $NAD^+$  5892, conformer #7) from the NCBI Pubchem database (<https://pubchem.ncbi.nlm.nih.gov/>, firstly accessed on 4 April 2023) to prepare ligand files using pdb-tools v2.4.8 (88). We used HADDOCK2.4 (89, 90) with default parameters optimized for protein-ligand docking analysis to obtain docking predictions for each ruff morph HSD17B2-T- $NAD^+$  ternary complex. To define the HSD17B2 residues at the interface, we generated two CNS-formatted restraints files (ambiguous and non-ambiguous distance) using GenTBL (<https://wenmr.science.uu.nl/gentbl/>). We determined known sites involved in testosterone and  $NAD^+$  binding regions according to the ruff HSD17B2 protein sequence from the NCBI conserved domain database ([https://www.ncbi.nlm.nih.gov/Structure/cdd/wrpsb.cgi?INPUT\\_TYPE=live&SEQUENCE=XP\\_](https://www.ncbi.nlm.nih.gov/Structure/cdd/wrpsb.cgi?INPUT_TYPE=live&SEQUENCE=XP_)



014797711.1). In the unambiguous restraint file, we listed residues S223 and Y236 of the catalytic tetrad as active sites for testosterone, while designating residues M224, A225, L230, S267, G268, Q274, Y303, G306 and A348 in the binding region as passive sites. Similarly, for NAD<sup>+</sup>, we indicated residues S223, Y236 and K240 of the catalytic tetrad as active sites and residues G93, D95, T96, G97, I98, L118, L141, D142, I143, N171, A172, G173, I174, V195, M221, S222, F269, T271, G272, I273 in the NAD<sup>+</sup> binding region as passive sites. Conversely, in the ambiguous restraint file, all previously mentioned sites were listed as passive. After molecular docking, we selected the model with the lowest internal energy from the top-scoring cluster in HADDOCK for subsequent analyses. Our analysis included further manual fitting of the cofactor using high-resolution x-ray experimental structures of other short-chain dehydrogenases (RCSB PDB IDs: 506X and 2O23). Manual fitting was minimized using protein preparation workflow in Maestro (Schrödinger Release 2024-4: Maestro, Schrödinger, LLC, New York, NY, 2024) with a maximum allowed root mean square deviation change of 0.6 Ångstrom, including all atoms. Finally, minimization was applied to refine hydrogens only. To assess variations in binding affinity towards the target ligands across the ruff morphs, we utilized the PRODIGY-LIG web tool (91, 92) for each allele-specific HSD17B2-T-NAD<sup>+</sup> ternary complex. We used PyMOL to visualize results of the molecular docking and examined atomic distances between the ligands and ‘NSYK’ catalytic tetrad sites.

#### Selection analysis

We used CODEML in the PAML package version 4.7.10 (93) to test for signatures of positive selection in the coding sequences (CDSs) of *HSD17B2* ruff morphs following recommendations outlined in ref. (94). We identified *HSD17B2* orthologs in other six Charadriiformes species (*Charadrius vociferus*, *Rissa tridactyla*, *Chroicocephalus ridibundus*, *Alca torda*, *Uria aalge*, *Limosa lapponica*) applying a reciprocal best-hit approach using pairwise BLAST searches. We used the perl scripts translatorX.pl, pal2nal.pl and FASTAtoPHYL.pl (bundled in <https://github.com/abacus-gene/paml-tutorial/tree/main/positive-selection>) to align the CDS with MAFFT, convert the alignments in codon data and convert the fasta alignment file to PHYLIP format. We then generated an unrooted gene tree using IQ-TREE v2.2.2.6 (95) and removed the branch lengths. To identify potential sites under positive selection, we ran a branch model using as foreground branches the *HSD17B2* CDS of the satellite and faeder haplotypes. The parameters for the null model were set as “model = 2, NSsites = 2, fix\_omega = 1 and omega = 1”, while the parameters for the alternative model were set as “model = 2, NSsites = 2, fix\_omega = 0 and omega = 0.5”. We compared the two models by likelihood ratio tests.

#### HSD17B2 expression plasmid cloning

We sourced seven expression plasmids each containing an *HSD17B2* sequence with ruff related mutant residues, based on vector backbone pIRES2-AcGFP1 (Clontech) from Genscript. Three plasmids expressed CDSs of known ruff variants from independent, faeder and satellite. Four additional plasmids (Var-1 to Var-4) expressed different combinations of the shared mutated sites in faeder and satellite *HSD17B2* CDSs to examine which of these shared mutations altered the catalytic activity of the faeder and satellite isozymes (Fig. 3A). The Var-1 insert contained only the L279F mutation because we wanted to test whether this mutation alone was sufficient to increase catalytic activity, as mutations to the corresponding residue in human HSD17B2 are known to have such an effect (41). Missense mutations at the corresponding position in the human HSD17B2 (L275E and L275M) increased catalytic activity ~5-fold for the testosterone to

androstenedione conversion relative to a non-mutated control (41). The Var-2 insert contained three mutations (A235S, L279F, I329T) to test whether these additional two mutations may have an additive effect, or be necessary in combination with L279F, for achieving higher catalytic activity. We selected A235S because it is immediately adjacent to the 'Y236' of the canonical 'NSYK' catalytic tetrad and binds to both steroid substrate and the cofactor, according to the conserved domains database. We selected I329T because the isoleucine is a conserved residue between human and ruff HSD17B2s and predicted to be in close vicinity of the cofactor. We did not include the I206T mutation in this insert because it is a common mutation in other bird species and in human as well, so we did not expect it would have a major effect on catalytic activity. The Var-3 insert contained three of the four shared mutated residues in satellite and faeder alleles, with L279 remaining as it is in the independent sequence, to test whether L279F is necessary for increased catalytic activity. Last, the Var-4 insert contained all four shared mutated residues, to test whether this specific combination is sufficient to reach the same levels of catalytic activity of satellite and faeder HSD17B2 isozymes.

Ruff-HSD17B2 inserts were synthesized *de novo* and subcloned by the company Genscript. The plasmid pIRES2-AcGFP1-hHSD17B2-MycHis (GenBank accession PP539712), originally designed to express human HSD17B2 as a C-terminally Myc-His tagged protein (41) served as the starting plasmid for the creation of the new vectors. The human HSD17B2 insert was replaced by the independent ruff HSD17B2 insert using restriction cloning with enzymes *Xho* I and *Sac* II to preserve the Myc-His tag in the vector backbone. The tag allowed for easy detection of the HSD17B2 proteins without the need of specific antibodies and without interfering with the catalytic activity or the protein localization to the membrane. Next, the remaining seven ruff HSD17B2 inserts were subcloned into the pIRES2-AcGFP1-IND\_HSD17B2-MycHis plasmid (GenBank accession PP539713) with *Xho* I and *Sac* II restriction cloning. We confirmed the plasmid sequences by Sanger sequencing. All plasmid accession numbers are listed in table S8.

#### Cell culture and transfection

We prepared HEK293 cell (ATCC) cultures in high glucose (4.5 g/L) Dulbecco's modified Eagle medium (DMEM; Gibco/Thermo Fisher Scientific) supplemented with 10 % fetal bovine serum superior (Sigma Aldrich) at 37 °C and 5 % CO<sub>2</sub> in a humidified atmosphere. Cells were frequently checked to be free of mycoplasma contamination using the MycoAlert™ mycoplasma detection kit (Lonza) and the MycoAlert™ assay control set (Lonza). We seeded cells with  $2 \times 10^6$  cells in T75 flasks (Nunc) and after 24 h transfected with 10 µg plasmid DNA per flask using X-treme 9 transfection reagent (Roche) in 1:3 ratio, according to the manufacturer's protocol. After 48 h, we detached the cells by trypsin/EDTA (Gibco), washed the harvested cell pellets once with PBS (pH 7.4), and stored cell pellet aliquots containing  $2 \times 10^6$  cells at -80 °C until use. As negative controls, we used non-transfected HEK293 cells.

#### Western blots

We prepared western blots as described previously in (41) with small adaptations. We resuspended cell aliquots ( $2 \times 10^6$  cells) in 200 µl reaction buffer (100 mM sodium phosphate, 1 mM EDTA, pH 7.6, cOmplete protease inhibitor (Roche)). We then mixed 40 µl of suspension with 10 µl of Laemmli buffer (300 mM Tris/HCl, 50 % glycerin, 10 % SDS, 0.05 % bromophenol blue, 25 % β-mercaptoethanol, pH 6.8) and heated the mixture at 95 °C for 15 min. We resolved 5 µl sample ( $4 \times 10^4$  cells) or 0.5 µl PageRuler Prestained Protein Ladder (Thermo Scientific) by

SDS-PAGE on 4-15 % TGX™ Precast Mini Protein Gels (BioRad) at 150 V. We transferred proteins to Immobilon FL PVDF membranes (Millipore) on a semi-dry Trans-blot apparatus from BioRad according to the manufacturer's instructions using a Towbin buffer (25 mM Tris, 192 mM glycine, 10 % SDS, 5 % MeOH) and by applying 20 V for 30 min. After blotting, we blocked membranes in 50 % Odyssey blocking buffer (PBS) (LI-COR) in PBS and incubated them overnight at 4 °C with 1:2000 diluted Mouse Anti-Myc clone 9B11 antibody (#2276, Cell Signaling) in 50 % Odyssey blocking buffer (PBS) in PBST (0.05 % Tween-20 in PBS). We washed blots three times with PBST and incubated them with goat anti-mouse IRDye 800CW (#926-32210) secondary antibodies (LI-COR) for 2 h at room temperature diluted 1:20000 in 50 % Odyssey blocking buffer (PBS) in PBST. After washing with PBS, we detected fluorescence signals by the Odyssey infrared imaging system (LI-COR) and analyzed band intensities (signal integration) using the Odyssey application software Image Studio Lite (LI-COR). We normalized band intensities of faeder, satellite, Var-1, Var-2, Var-3 and Var-4 HSD17B2 proteins to the independent HSD17B2 protein intensity and then used the resulting values for normalization of enzymatic activity data (fig. S11). We performed the protein quantification experiments in duplicates.

### Enzyme kinetics

We measured the conversion of radiolabeled [1,2,6,7-3H (N)] testosterone (ARC) to [1,2,6,7-3H (N)] delta-4 androstenedione. The reaction mixture of 500 µl contained 1 or  $2 \times 10^3$  transfected HEK293 cells, 0.75 mM cofactor NAD<sup>+</sup> (Serva), 10 nM radiolabeled testosterone, and 0 to 2.5 µM unlabeled testosterone in reaction buffer (100 mM sodium phosphate, 1 mM EDTA, pH 7.6, and cOmplete protease inhibitor). We incubated reaction samples for 15 min at 29.5 °C. After termination of the reaction by the addition of stop solution (0.25 M ascorbic acid, 1 % acetic acid in MeOH) we extracted steroids on reversed phase Strata C-18E SPE cartridges (Phenomenex) using a vacuum manifold and negative pressure. We conditioned cartridges twice with 1 ml MeOH and equilibrated with two times 1 ml water. We applied the samples to the cartridges, washed with 0.5 ml water, and eluted steroids with two times 200 µl MeOH. We performed the separation of substrate and product by isocratic HPLC (Beckman Coulter) using the solvent water/acetonitrile (57/43, v/v) on a reversed phase column (LUNA 5 µm C18(2) 125 mm x 4 mm, Phenomenex) at a flow rate of 1 ml/min. We detected tritiated steroids via an online radioactivity monitor (LB506D, Berthold) after mixing them 1:1 with scintillation solution (Quicksafe Flow 2, Zinsser). We calculated the percentage of steroid conversion from integrated substrate and product peaks using the 32Karat software (Beckman Coulter). We performed activity experiments in triplicates. To determine conversion rates, we normalized expression of HSD17B2 proteins based on their anti-Myc signals from Western blots. As a reference we used the signal expression of independent HSD17B2. As the enzyme was not purified, we were unable to establish the enzyme concentrations that are needed to calculate catalytic efficiency. Instead, we calculated  $K_M$  and  $v_{max}$  values from the normalized conversion of testosterone to delta-4 androstenedione by fitting the data to the Michaelis-Menten equation using the GraphPad Prism 10.2.0 software and plotted summarized results with R.

### Statistical analysis and visualization

Pipelines used for allele-specific expression and differential gene expression data analysis were constructed with Snakemake (96). Statistical analysis and data visualization were conducted

using R v4.3.1 (R Core Team, 2019) in RStudio v.2023.09.1. A complete list of the scripts and R packages employed in our analyses is available at Zenodo DOI:10.5281/zenodo.11032422.

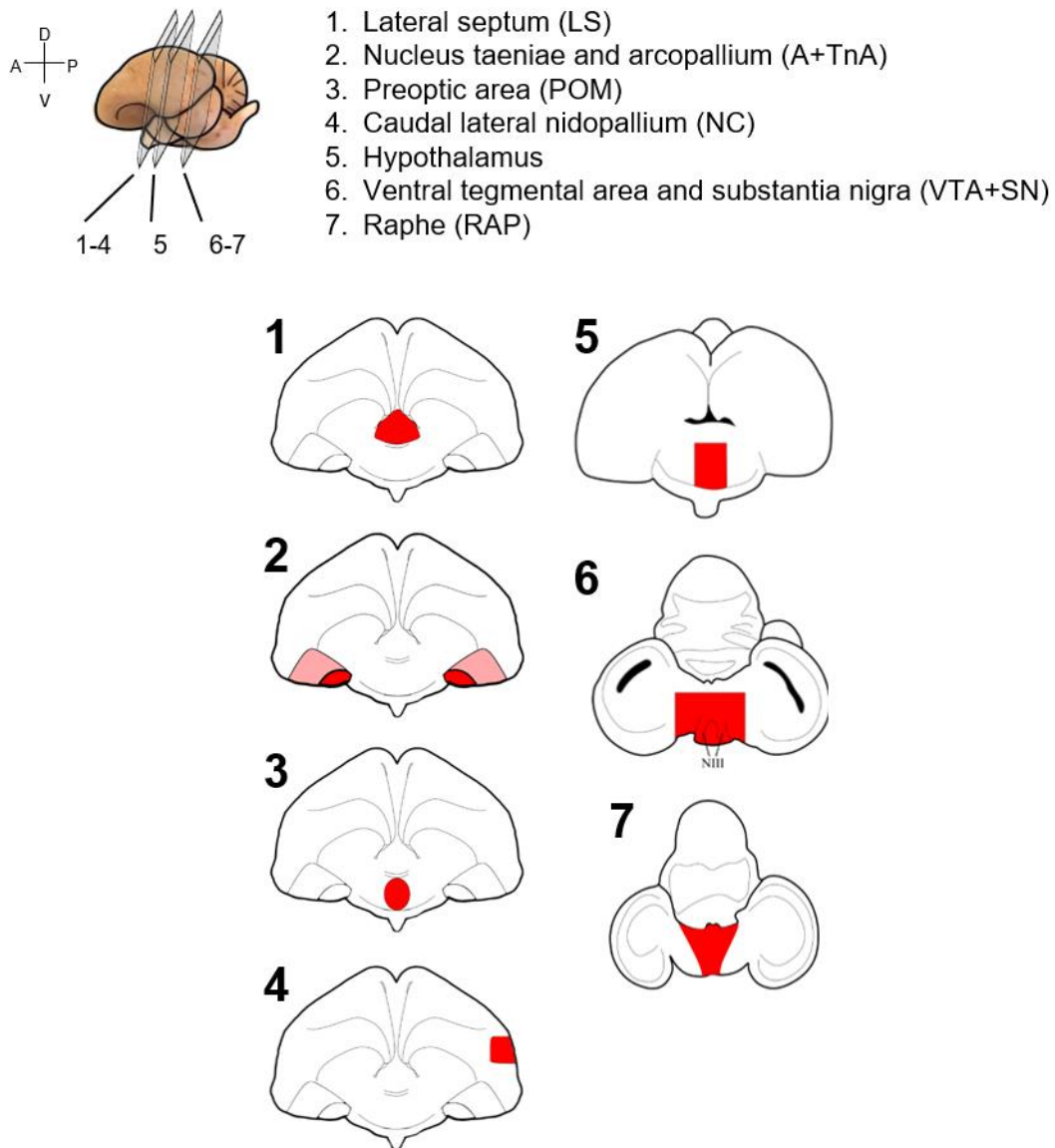


**Fig. S1. Location of microdissected brain nuclei in the ruff brain (*Calidris pugnax*) for RNA-Seq**

Sagittal depiction of a male ruff brain shows the approximate locations of sampled nuclei numbered 1-7 (top left). Drawings of representative coronal sections illustrate the locations of microdissected samples and targeted brain nuclei (colored). Brain nuclei that are adjacent to each other on the same section are shown in different colors (red; nucleus taeniae; pink, arcopallium). Orientation is noted with anteroposterior and dorsoventral axes. Abbreviations: A, anterior; P, posterior, D, dorsal; V, ventral; NIII, oculomotor cranial nerve. Tracings were drawn based on images of a nissl-stained male ruff brain.

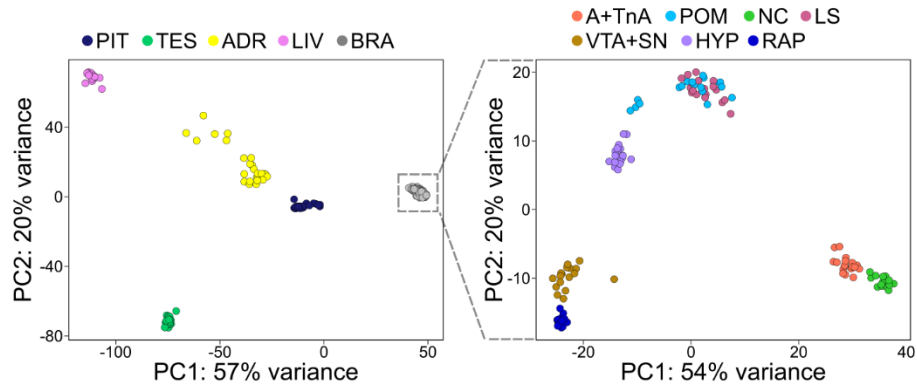


**Fig. S2. Principal component analysis of RNA-Seq samples from brain and organs**

Principal component analysis of expression profiles for samples from brain areas and organs ( $n = 229$ ). Samples clustered by organ (left) with most brain samples also clustering by brain area (right), except for preoptic area and lateral septum, two adjacent brain areas, clustering together. Abbreviations: PIT, pituitary; TES, testes; ADR, adrenals; LIV, liver; BRA, brain; VTA+SN, ventral tegmental area and substantia nigra; HYP, hypothalamus; LS, lateral septum; A+TnA, arcopallium and nucleus taeniae; POM, preoptic area; NC, caudal nidopallium; RAP, raphe.

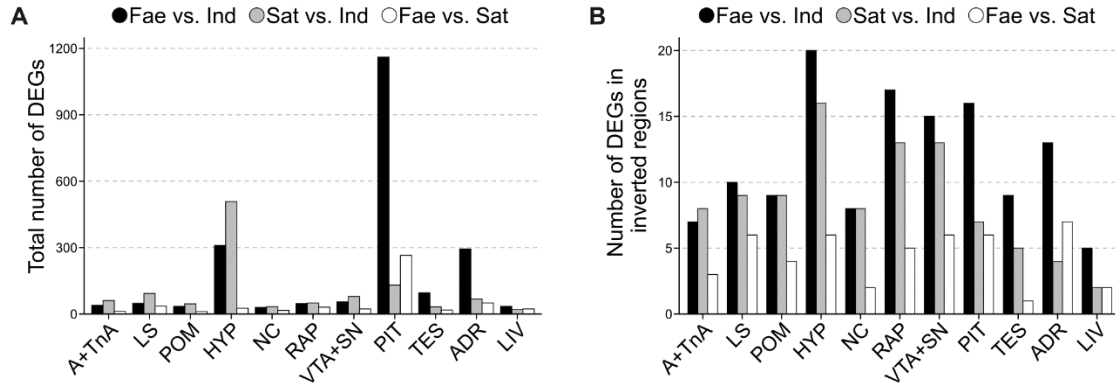


**Fig. S3. Tissue-specific number of differentially expressed genes in the ruff genome and inversion region**

(A) Number of differentially expressed genes across the entire genome and (B) in the inversion region for pairwise comparisons between morphs. For the genome, we counted the total number of differentially expressed genes in each dataset from the tissue-level analysis and plotted these by tissue type and pairwise morph comparison. For the inversion region, we counted the number of inversion genes within the datasets shown in (A).  $n = 229$  samples. Abbreviations: A+TnA, arcopallium and nucleus taeniae; LS, lateral septum; POM, preoptic area; HYP, hypothalamus; NC, caudal nidopallium; RAP, raphe; VTA+SN, ventral tegmental area and substantia nigra; PIT, pituitary; TES, testes; ADR, adrenals; LIV, liver; Fae, faeder; Sat, satellite; Ind, independent.

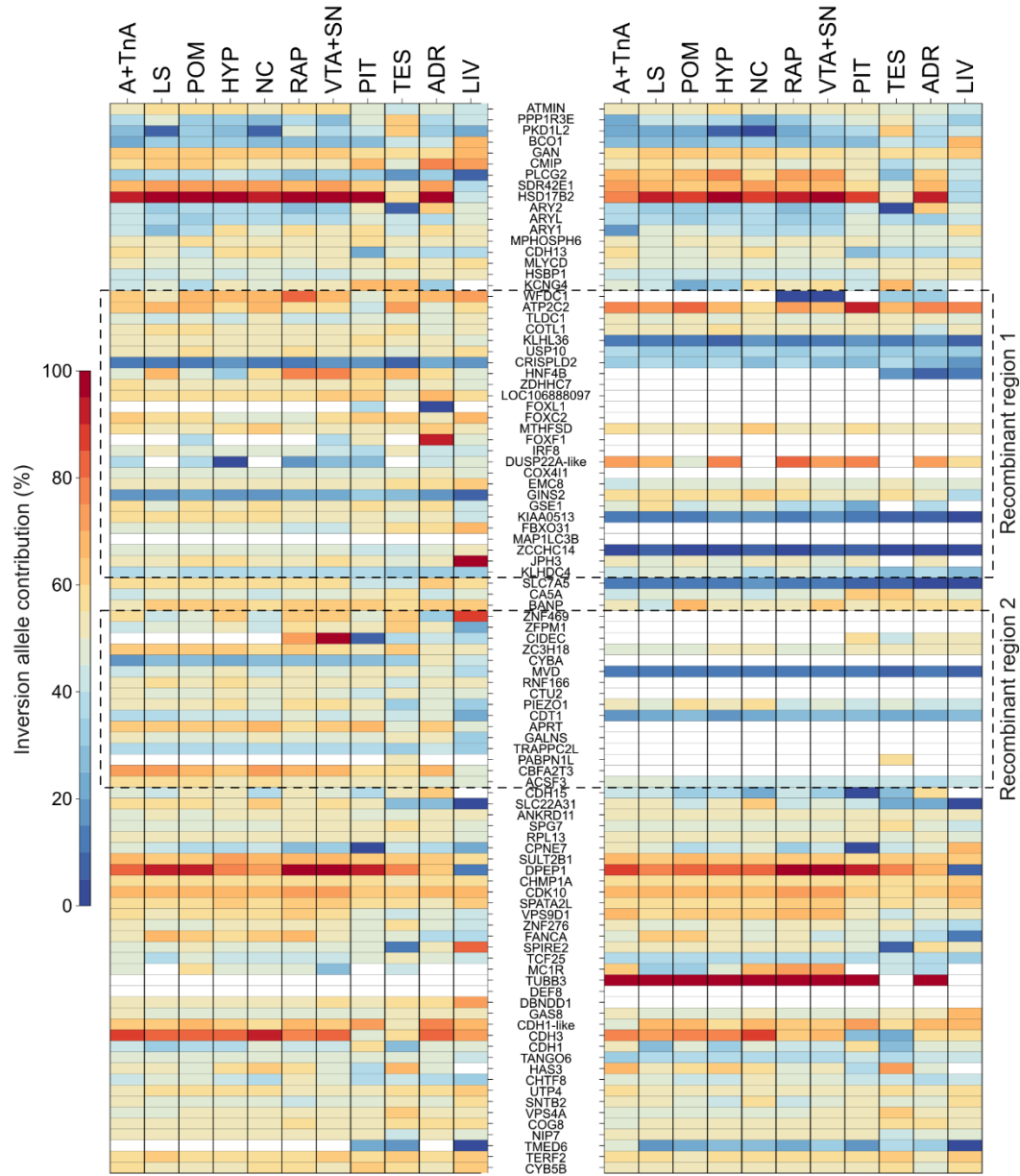


**Fig. S4. Faeder and satellite allele-specific expression of loci in the inversion region across organs and brain areas**

Heatmap depicts the extent of allele specific expression of all annotated genes located in the inversion region in faeders (left) and satellites (right), the two morphs that are obligate heterozygotes in this genomic area. The contribution of the inversion allele is expressed as percentage of total expression in each tissue. Each column is a tissue, each row is a gene. Genes are ordered top to bottom according to genomic location in the ancestral independent allele. White background denotes either the gene was not expressed or a SNP is not available in the gene to allow measuring allele-specific expression. Areas in the satellite haplotype that underwent recombination with an independent allele are boxed and labeled ‘Recombinant region 1’ and



‘Recombinant region 2’. Abbreviations as in fig. S3. Sample sizes: faeders:  $n = 63$  samples; satellites:  $n = 63$  samples, for further details see table S4.

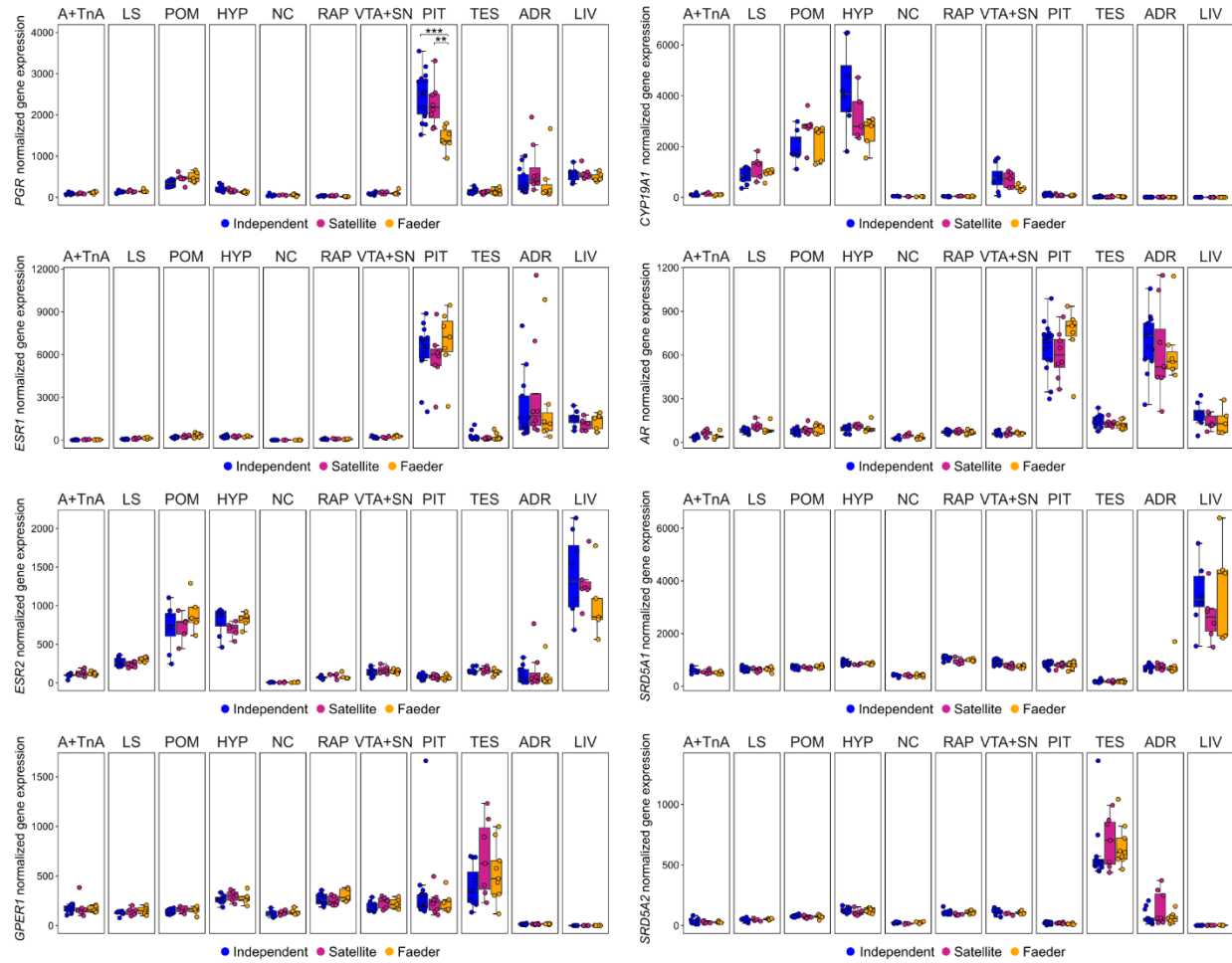


**Fig. S5. Expression of sex steroid receptor and enzyme encoding genes by tissue and morph**  
 Variation in gene expression between male ruff morphs for five sex steroid receptors (*PGR*, *ESR1*, *ESR2*, *GPER1*, *AR*) and three androgen pathway enzymes responsible for metabolizing testosterone into either estradiol (*CYP19A1*) or dihydrotestosterone (*SRD5A1*, *SRD5A2*) across brain areas and organs. The only statistically clear morph difference among sex steroid receptors was in *PGR* where faeders had lower pituitary expression compared to both independents and satellites (faeder vs. independent,  $p = 0.00004$ ; faeder vs. satellite,  $p = 0.0106$ ). These results are in agreement with ref (24).  $p$ -values for morph differences were Benjamini-Hochberg corrected. See table S7 for gene names and descriptions. Abbreviations as in fig. S3.

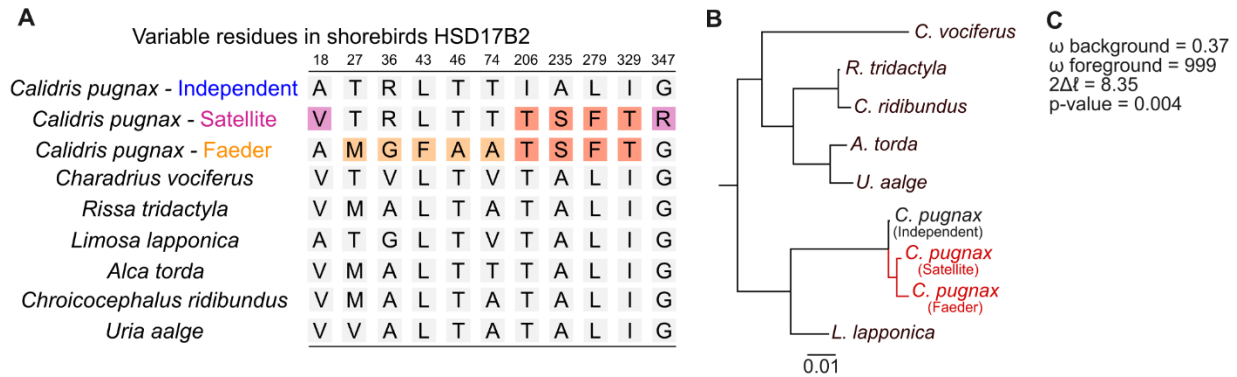


**Fig. S6. Evidence for positive selection at *HSD17B2* protein coding sequences in satellites and faeders**

(A) Sequence alignment of variable sites in *HSD17B2* across the Charadriiformes order that differ in at least one inversion haplotype compared to the ancestral haplotype. Within the ligand-binding regions (positions 93-348), three out of four mutated residues that are linked with increase in enzymatic activity are restricted to the ruff inversion haplotypes (A235S, L279F, I329T), and one additional mutation is only in the satellite haplotype (G347R, purple). Relative to the ancestral (independent) allele, mutated residues shared by satellite and faeder alleles are in orange, mutated residues only in faeder alleles are in yellow, and those only in satellite are in purple. Position numbers from XP\_014797711.1. (B) *HSD17B2* gene tree based on its protein coding sequence; satellite and faeder are shown in red. (C) CODEML results under the branch model using the inversion haplotype lineage as foreground branch.

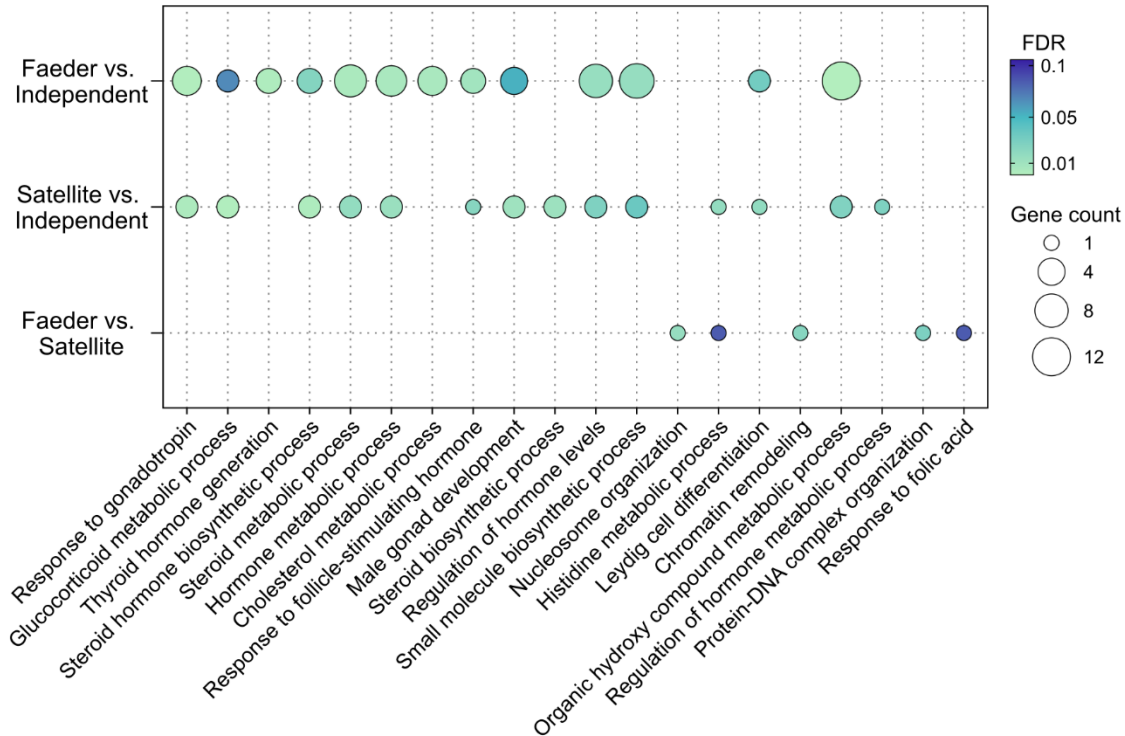


**Fig. S7. Testicular expression of genes with gene ontology terms relevant to steroidogenesis**

Over-representation analysis (ORA) showing the top 15 non-redundant gene ontology (GO) terms in testes for all pairwise morph comparisons (FDR < 0.1). Lists of differentially expressed genes from the faeder vs. independent and satellite vs. independent comparison had more genes associated with ‘Steroid hormone biosynthetic process’ and ‘Hormone metabolic processes’ than expected (first and second rows), and included many genes across the 15 top GO terms for putative differences in reproductive processes. In contrast, the faeder vs. satellite comparison had no over-representation in ‘Steroid hormone biosynthetic process’ and ‘Hormone metabolic processes’ GO terms and only five genes in GO terms but these were not explicitly related to steroidogenesis.

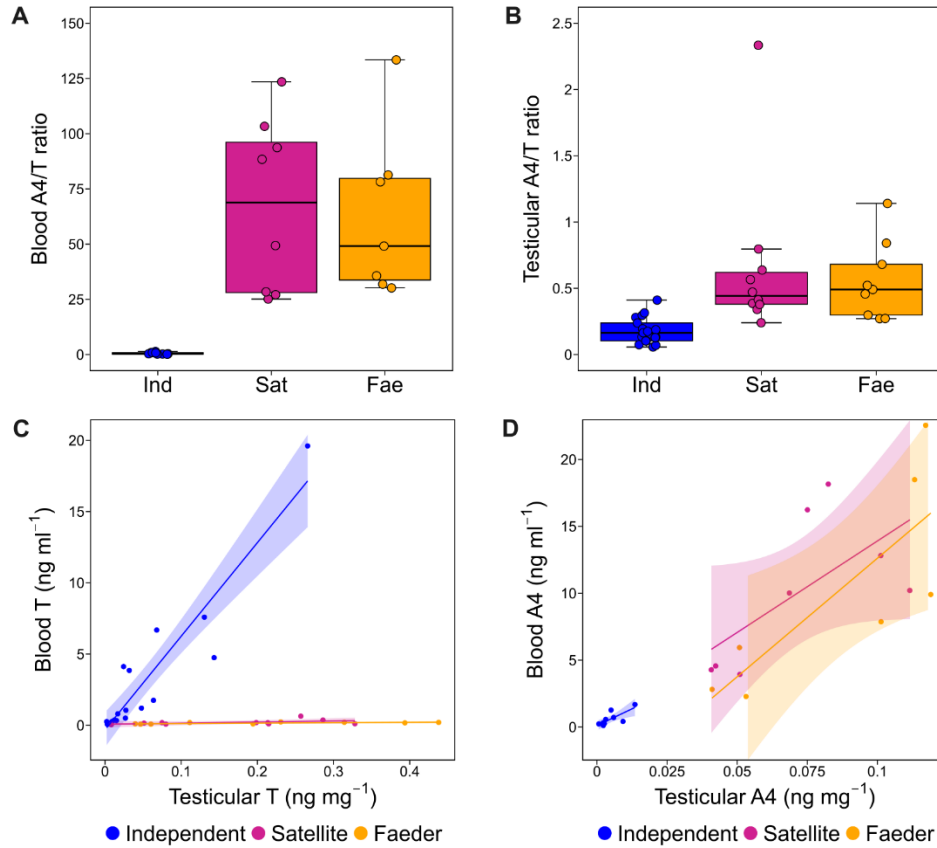


**Fig. S8. Morph comparisons and relationships between blood and testicular androgens**

Satellites and faeders had greater androstenedione to testosterone ratios in (A) the blood and (B) testes compared to independents. We detected clear differences among morphs in both tissues: blood (Kruskal-Wallis  $H(2) = 17.308$ ,  $p < 0.001$ ,  $n = 25$ ; testes (Kruskal-Wallis  $H(2) = 20.968$ ,  $p < 0.001$ ,  $n = 36$ ). Satellites and faeders had higher ratios compared to independents in blood and testes (Wilcoxon-tests with Bonferroni adjustment: independent vs. satellite,  $p < 0.001$ ; independent vs. faeder,  $p < 0.001$ ), but there were no clear differences between satellites and faeders ( $p = 1$ ). (C) In independents, circulating and testicular levels of testosterone were strongly correlated ( $r = 0.93$ ,  $p < 0.001$ ,  $n = 17$ ), but this was not the case for satellites ( $r = 0.43$ ,  $p = 0.33$ ,  $n = 10$ ) or faeders ( $r = 0.65$ ,  $p = 0.1$ ,  $n = 9$ ). (D) Similarly, all morphs showed a positive relationship between circulating and testicular androstenedione, but the relationship was weaker in satellites and faeders. See table S3 for details. (C, D) Spearman correlation coefficients. Abbreviations: A4, androstenedione; T, testosterone.

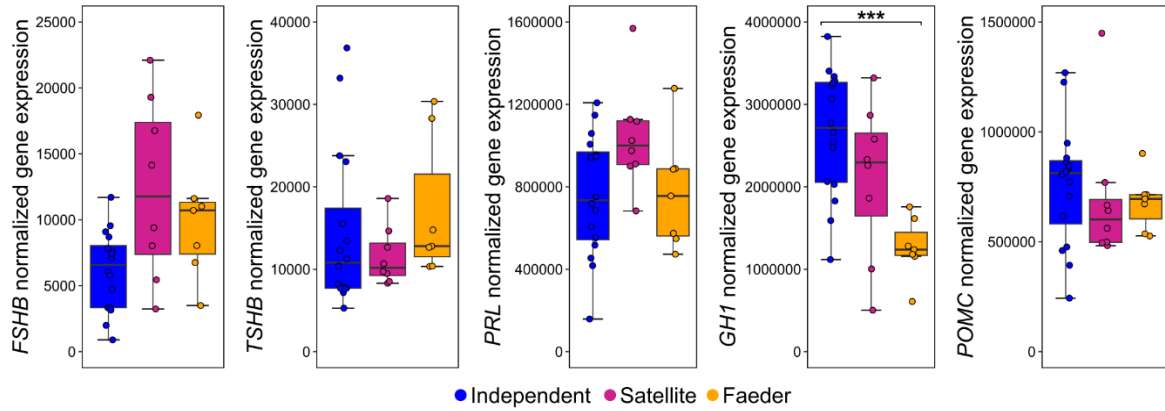


**Fig. S9. Morph-specific expression of genes encoding main anterior pituitary hormones**

Pituitaries had the largest number of differentially expressed genes than any other tissue and genes encoding major anterior pituitary hormones were expressed at high abundance in this tissue. There was only one differentially expressed gene among five genes encoding major anterior pituitary hormones: *GH1*, which encodes growth hormone 1 (GH1). Faeders had lower *GH1* expression than independents (Benjamini-Hochberg corrected  $p = 0.0006$ ). The gene encoding luteinizing hormone is not shown because it is not an annotated gene in the ruff genome and previous efforts to locate it were not successful (25). Each plot,  $n = 31$ . See table S7 for gene names and descriptions. independent (blue), satellite (pink), faeder (yellow).

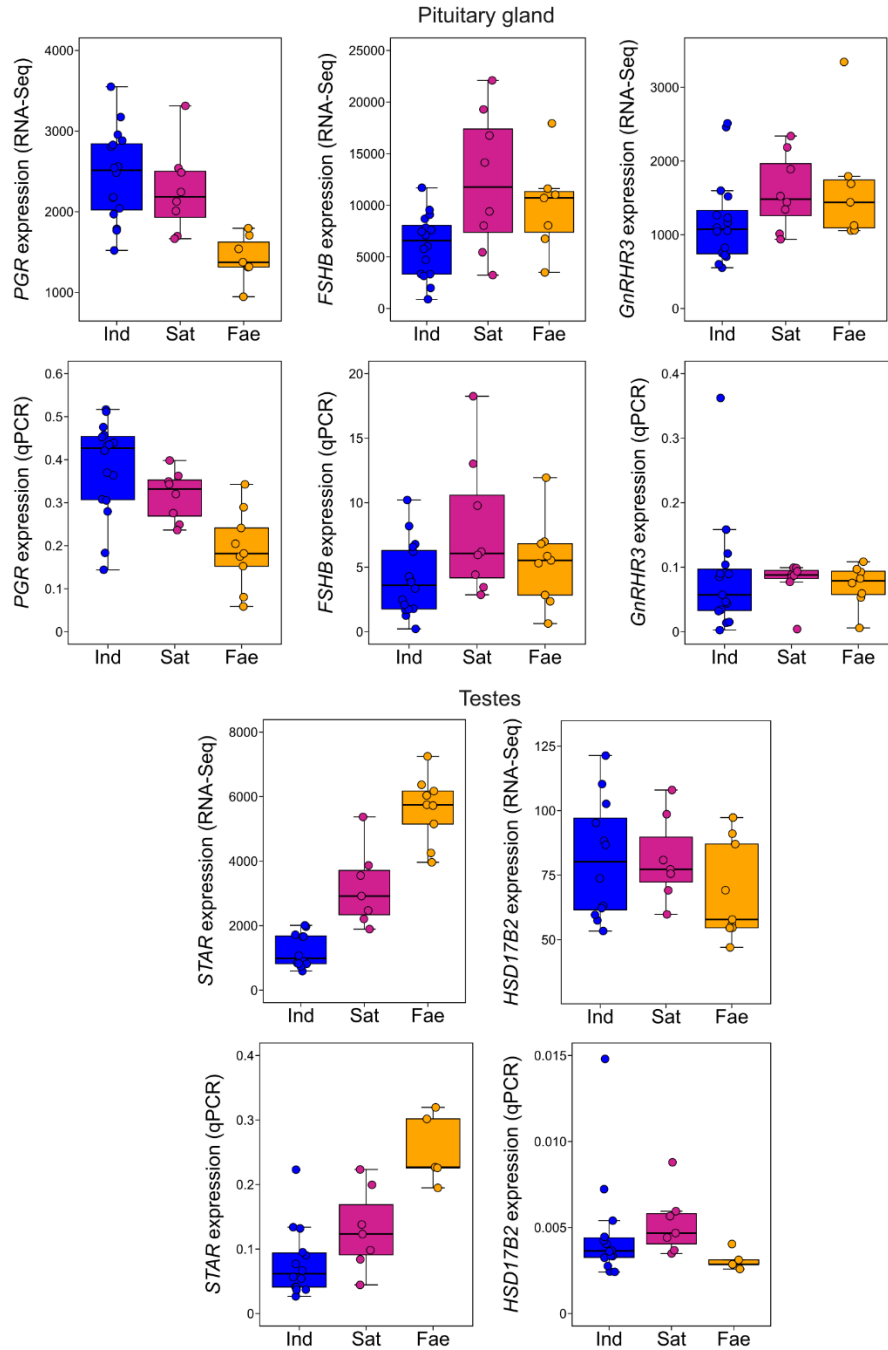


**Fig. S10. Validation of differentially expressed genes by quantitative PCR**

Validation of RNA-Seq results using expression results of five genes expressed in pituitary or testes (pituitary: *PGR*, *FSHB*, *GnRHR3*; testes: *STAR* and *HSD17B2*). RNA-Seq data are from this study whereas data from quantitative PCRs are from refs (24, 25)). For both ‘Pituitary’ and ‘Testes’, top row is RNA-Seq data (pituitaries, n = 31; testes, n = 28), and bottom rows is qPCR data (pituitaries, n = 33; testes, n = 26). See table S7 for gene names and descriptions. Abbreviations: Fae, faeder; Sat, satellite; Ind, independent.

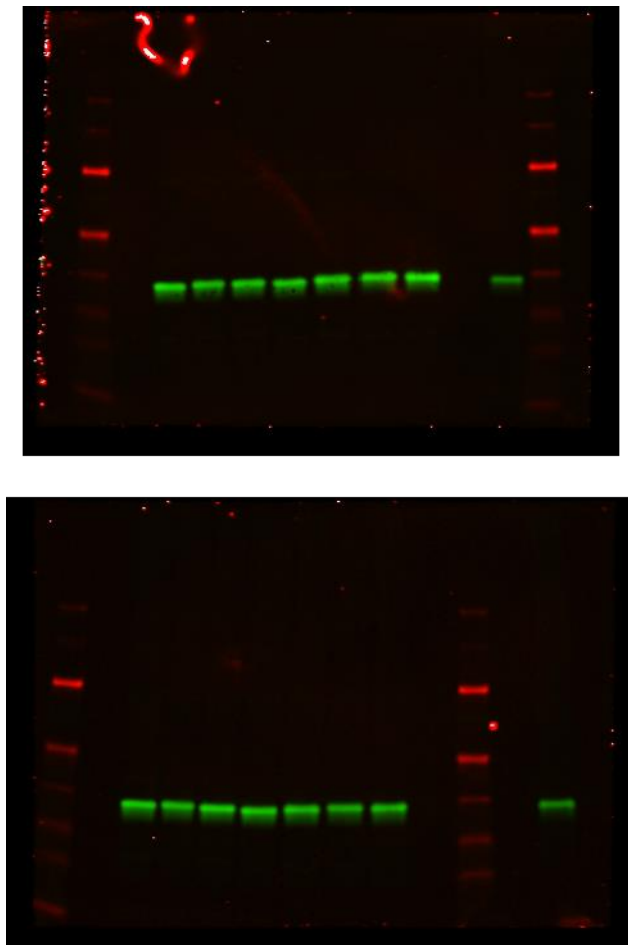


**Fig. S11. Western blots**

Western blots of HSD17B2 expressed in transfected cells used to normalize enzymatic activity. Protein quantification was performed in duplicates. Lanes in the first blot (top): marker, buffer, Ind, Sat, Fae, Var-1, Var-2, Var-3, Var-4, buffer, human HSD17B2, marker. Lanes in the second blot (bottom): marker, buffer, Ind, Sat, Fae, Var-1, Var-2, Var-3, Var-4, buffer, marker, buffer, human HSD17B2. We normalized band intensities of faeder, satellite, Var-1, Var-2, Var-3 and Var-4 HSD17B2 proteins to the independent HSD17B2 protein intensity and then used the resulting values for normalization of enzymatic activity data shown in Fig. 3, E and F. For details of each ruff HSD17B2 protein sequence see Fig. 3A and table S8.



Comparison	Pvalue	Padjust	95% Confidence interval	Odds_ratio
Fae vs. Ind - ADR	1.41E-15	7.83E-15	17.85222 - 69.87327	36.54846
Fae vs. Ind - BLO	0.0007351	0.000895903	2.137413 - 14.284305	6.111831
Fae vs. Ind - TES	3.61E-09	8.17E-09	8.51879 - 41.18769	19.88363
Fae vs. Ind - HYP	1.05E-15	6.83E-15	8.318017 - 24.575162	14.6003
Fae vs. Ind - LIV	2.29E-06	3.44E-06	8.344316 - 75.869691	28.22529
Fae vs. Ind - LS	1.71E-13	8.34E-13	21.22372 - 105.25556	49.38911
Fae vs. Ind - NC	6.02E-12	2.00E-11	24.81095 - 161.00178	66.3498
Fae vs. Ind - PIT	0.00118	0.001394545	1.428270 - 4.555865	2.628581
Fae vs. Ind - POM	4.15E-13	1.80E-12	25.28669 - 144.36005	63.20684
Fae vs. Ind - RAP	2.20E-16	2.15E-15	56.13281 - 223.50361	113.3368
Fae vs. Ind - A+TnA	3.46E-09	8.17E-09	13.79451 - 90.82550	38.02623
Fae vs. Ind - VTA+SN	2.20E-16	2.15E-15	36.24618 - 142.13960	73.538
Sat vs. Ind - ADR	0.0001109	0.000139519	4.64505 - 52.24399	18.27478
Sat vs. Ind - BLO	6.39E-05	8.31E-05	5.392685 - 63.683264	21.60835
Sat vs. Ind - TES	9.46E-07	1.54E-06	10.03843 - 92.77354	34.12466
Sat vs. Ind - HYP	3.73E-08	6.93E-08	3.489076 - 11.246874	6.451342
Sat vs. Ind - LIV	0.006704	0.007262667	2.017385 - 78.034540	18.20208
Sat vs. Ind - LS	3.77E-09	8.17E-09	8.482586 - 41.255104	19.8283
Sat vs. Ind - NC	1.41E-11	4.23E-11	22.10437 - 138.86470	58.36531
Sat vs. Ind - PIT	1.10E-05	1.59E-05	3.966666 - 22.897225	10.36284
Sat vs. Ind - POM	6.14E-12	2.00E-11	18.28534 - 97.54701	44.37985
Sat vs. Ind - RAP	2.20E-16	2.15E-15	31.42815 - 135.00443	66.86275
Sat vs. Ind - A+TnA	3.40E-09	8.17E-09	10.57655 - 58.37811	26.49926
Sat vs. Ind - VTA+SN	1.03E-15	6.83E-15	18.34229 - 72.51811	37.674
Fae vs. Sat - ADR	1.29E-08	2.52E-08	11.27738 - 71.20687	30.59032
Fae vs. Sat - BLO	0.309	0.309	0.06817434 - 16.58778965	2.776324
Fae vs. Sat - TES	0.09741	0.099973421	0.246409 - 67.738662	10.39788
Fae vs. Sat - HYP	7.10E-09	1.46E-08	17.42419 - 144.87271	54.30124
Fae vs. Sat - LIV	0.008821	0.009297811	1.746361 - 65.421027	15.59448
Fae vs. Sat - LS	6.07E-08	1.08E-07	11.90046 - 90.54371	35.86047
Fae vs. Sat - NC	0.003971	0.004554971	2.651217 - 108.654730	24.36072
Fae vs. Sat - PIT	0.004784	0.005330743	1.453398 - 9.408653	4.103551
Fae vs. Sat - POM	3.83E-07	6.49E-07	20.82883 - 392.90232	98.71674
Fae vs. Sat - RAP	1.06E-06	1.65E-06	9.815494 - 91.340202	33.47114
Fae vs. Sat - A+TnA	4.74E-05	6.37E-05	9.521011 - 225.991820	55.50883
Fae vs. Sat - VTA+SN	3.62E-09	8.17E-09	19.66399 - 170.70502	62.36419
Fae vs. Ind - Phenotype	2.20E-16	2.15E-15	5.324305 - 12.452562	8.145178
Sat vs. Ind - Phenotype	2.22E-12	8.66E-12	3.518201 - 8.631744	5.556502
Fae vs. Sat - Phenotype	4.40E-05	6.13E-05	1.778529 - 5.019421	3.048701

**Table S1. Enrichment of differentially expressed genes in the inversion region**

Enrichment was examined for differentially expressed genes from pairwise morph comparisons in each tissue and at the morph-level ('Phenotype') with a Fisher test and the computed p-values were corrected for multiple testing using the Benjamini-Hochberg method. Abbreviations: Fae, faeder;

Sat, satellite; Ind, independent; PIT, pituitary; TES, testes; ADR, adrenals; LIV, liver; BLO, blood; VTA+SN, ventral tegmental area and substantia nigra; HYP, hypothalamus; LS, lateral septum; A+TnA, arcopallium and nucleus taeniae; POM, preoptic area; NC, caudal nidopallium; RAP, raphe.

<i>Genes involved with steroid transport</i>							
Gene symbol	Base mean	log2FC	lfcSE	pvalue	padj	Gene description	Source
<i>ABCG2</i>	8.41	0.310	0.25	1.03E-03	1.66E-02	ATP-binding cassette, sub-family G	SRS_PHEN_FI
<i>SLCO2B1</i>	1754.39	-0.186	0.09	6.35E-04	1.15E-02	Solute carrier organic anion transporter family, member	SRS_PHEN_FI
<i>ABCB10</i>	1750.21	-0.247	0.06	1.72E-06	1.13E-04	ATP binding cassette subfamily B member 10	SRS_PIT_FI
<i>ABCC10</i>	1194.02	0.139	0.05	7.68E-04	1.66E-02	ATP binding cassette subfamily C member 10	SRS_PIT_FI
<i>SLCO2B1</i>	1753.55	-1.477	0.27	5.52E-10	1.04E-07	solute carrier organic anion transporter family member 2B1	SRS_PIT_FI
<i>SLCO2B1</i>	1753.55	-1.918	0.30	4.01E-12	6.48E-09	solute carrier organic anion transporter family member 2B1	SRS_PIT_FS
<i>Endoplasmic reticulum markers</i>							
Gene symbol	Base mean	log2FC	lfcSE	pvalue	padj	Gene description	Source
<i>COL1A2</i>	20482.94	-0.614	0.34	1.26E-04	3.50E-02	collagen type I alpha 2 chain	SRS_ADR_FI
<i>RTN4</i>	20815.35	0.121	0.04	8.15E-06	4.19E-03	reticulon 4	SRS_ADR_FI
<i>COL1A2</i>	20482.94	-0.746	0.38	1.69E-05	1.09E-02	collagen type I alpha 2 chain	SRS_ADR_FS
<i>RRBP1</i>	9070.95	0.307	0.12	5.44E-05	6.93E-03	ribosome binding protein 1	SRS_HYP_FI
<i>SCD</i>	7215.25	0.253	0.15	3.39E-04	2.39E-02	stearoyl-CoA desaturase	SRS_HYP_FI
<i>RTN4IP1</i>	1192.90	-0.149	0.06	1.35E-03	4.23E-02	reticulon 4 interacting protein 1	SRS_HYP_SI
<i>CALU</i>	609.64	0.111	0.07	3.57E-03	3.94E-02	calumenin	SRS_PHEN_FI
<i>COL1A2</i>	2924.69	-0.545	0.13	7.86E-07	6.29E-05	collagen type I alpha 2 chain	SRS_PHEN_FI
<i>RCN1</i>	1248.07	-0.102	0.05	2.06E-03	2.64E-02	reticulocalbin 1	SRS_PHEN_FI
<i>SCD5</i>	18306.90	-0.127	0.04	1.03E-04	3.02E-03	stearoyl-CoA desaturase 5	SRS_PHEN_FI
<i>COL1A2</i>	2924.69	-0.164	0.14	3.39E-03	4.20E-02	collagen type I alpha 2 chain	SRS_PHEN_SI
<i>RTN4IP1</i>	1139.14	-0.101	0.04	5.23E-04	1.17E-02	reticulon 4 interacting protein 1	SRS_PHEN_SI
<i>CALR</i>	14010.43	0.310	0.21	2.10E-03	3.45E-02	calreticulin	SRS_PIT_FI
<i>CANX</i>	13144.42	0.220	0.15	3.53E-03	4.95E-02	calnexin	SRS_PIT_FI
<i>COL1A2</i>	2290.89	-0.647	0.53	1.23E-03	2.34E-02	collagen type I alpha 2 chain	SRS_PIT_FI
<i>LOC106886953</i>	2243.69	0.491	0.08	5.79E-10	1.07E-07	lanosterol 14-alpha demethylase	SRS_PIT_FI
<i>P4HB</i>	5987.24	0.281	0.09	2.98E-05	1.24E-03	prolyl 4-hydroxylase subunit beta	SRS_PIT_FI
<i>PDI43</i>	33372.46	0.730	0.14	2.45E-08	2.97E-06	protein disulfide isomerase family A member 3	SRS_PIT_FI
<i>RRBP1</i>	5826.40	0.226	0.15	3.26E-03	4.70E-02	ribosome binding protein 1	SRS_PIT_FI
<i>LOC106886953</i>	2243.69	0.293	0.13	1.08E-04	1.21E-02	lanosterol 14-alpha demethylase	SRS_PIT_FS
<i>PDI43</i>	33372.46	0.348	0.21	1.15E-04	2.16E-02	protein disulfide isomerase family A member 3	SRS_PIT_SI
<i>SEC family proteins</i>							
Gene symbol	Base mean	log2FC	lfcSE	pvalue	padj	Gene description	Source
<i>SEC61A2</i>	3048.02	-0.099	0.04	2.24E-04	1.75E-02	SEC61 translocon subunit alpha 2	SRS_HYP_FI
<i>SECISBP2L</i>	6891.30	0.138	0.09	8.47E-04	4.41E-02	SECIS binding protein 2 like	SRS_HYP_FI
<i>SEC22B</i>	7070.02	-0.127	0.04	6.32E-04	2.68E-02	SEC22 homolog B, vesicle trafficking protein	SRS_HYP_SI
<i>SEC61A2</i>	3048.02	-0.121	0.04	3.91E-04	2.00E-02	SEC61 translocon subunit alpha 2	SRS_HYP_SI
<i>SEC16B</i>	119.52	0.253	0.25	2.15E-03	2.74E-02	SEC16 homolog B, endoplasmic reticulum export factor	SRS_PHEN_FI
<i>SEC13</i>	3087.56	0.066	0.02	1.24E-03	2.33E-02	SEC13 homolog, nuclear pore and COPII coat complex component	SRS_PHEN_FS
<i>SEC22C</i>	294.32	0.150	0.06	1.62E-04	5.18E-03	SEC22 homolog C, vesicle trafficking protein	SRS_PHEN_SI
<i>SEC16B</i>	18.31	0.627	0.92	7.42E-04	4.62E-02	SEC16 homolog B, endoplasmic reticulum export factor	SRS_PIT_FS

**Table S2. No evidence for altered testicular expression of steroid transport or endoplasmic reticulum marker genes**

We surveyed all 36 lists of differentially expressed genes for genes putatively involved with steroid transport (11 genes), known endoplasmic reticulum markers (17 genes from ref. (97)) and SEC genes that control transport of vesicles in secretory pathways and only found differentially expressed genes in the morph model of analysis ‘PHEN’, adrenal glands ‘ADR’, pituitaries ‘PIT’, hypothalamus ‘HYP’, but not in testes. Source refers to the differentially expressed genes list,

containing in its name the tissue and pairwise morph comparison faeder vs. independent 'FI', satellite vs. independent 'SI', faeder vs. satellite 'FS'.

*Independents*

	Testes T	Plasma A4	Plasma T
Testes A4	<b>0.93</b> <b>5.33E-16</b> (17)	<b>0.81</b> <b>8.00E-03</b> (10)	<b>0.86</b> <b>5.33E-16</b> (17)
Testes T		<b>0.93</b> <b>1.56E-04</b> (10)	<b>0.93</b> <b>5.33E-16</b> (17)
Plasma A4			<b>0.97</b> <b>5.33E-16</b> (10)

*Satellites*

	Testes T	Plasma A4	Plasma T
Testes A4	<b>0.88</b> <b>0.011</b> (10)	0.71 0.173 (8)	0.32 0.442 (10)
Testes T		0.50 0.432 (8)	0.43 0.327 (10)
Plasma A4			0.31 0.462 (8)

*Faeaders*

	Testes T	Plasma A4	Plasma T
Testes A4	<b>0.90</b> <b>0.01</b> (9)	0.79 0.10 (7)	0.48 0.19 (9)
Testes T		<b>0.89</b> <b>0.04</b> (7)	0.65 0.10 (9)
Plasma A4			0.71 0.11 (7)

**Table S3. Correlation matrices for testosterone and androstenedione in plasma and testes**

Morph-specific Spearman correlation coefficients and p-values for relationships among testosterone (T) and androstenedione (A4) in testes and plasma from blood. p-values were Benjamini-Hochberg corrected for multiple tests within each morph. Numbers in parentheses indicate number of birds. Numbers in bold indicate corrected  $p < 0.05$ .

<b>Tissue</b>	<b>Independent</b>	<b>Satellite</b>	<b>Faeder</b>	<b>Total</b>
A+TnA	8	5	5	18
LS	8	5	5	18
POM	8	5	5	18
HYP	8	5	5	18
NC	6	4	5	15
RAP	8	5	5	18
VTA+SN	8	5	5	18
PIT	16	8	7	31
TES	12	7	9	28
ADR	13	8	7	28
LIV	8	6	5	19
Totals	103	63	63	229

**Table S4. RNA-Seq sample sizes for organs and brain areas by morph**

We collected 36 birds for RNA-Seq tissue sampling. The sample sizes for each organ and brain area are shown by morph, with corresponding totals. Abbreviations: A+TnA, arcopallium and nucleus taeniae; LS, lateral septum; POM, preoptic area; HYP, hypothalamus; NC, caudal nidopallium; RAP, raphe; VTA+SN, ventral tegmental area and substantia nigra; PIT, pituitary; TES, testes; ADR, adrenals; LIV, liver.

Category	Behavior	Description
<b>Aggression</b>	<i>Peck</i>	The bird pecks a receiver, beak is close to horizontal. The pecking bird may be in the forward posture prior the pecking event.
	<i>Fight</i>	The bird participates in mutual agonistic behavior with another bird, with contact. The bird may jump to the rival with the wings open.
	<i>Chase</i>	The bird charges at another bird and the chased bird runs away from the bird that is charging.
	<i>Forward</i>	Body horizontal to the ground or points slightly down. Bill points forward or might be slightly pointing down. Tail may be spread or not and the bird often bill thrusts by moving the head rapidly forward and backwards. Could be walking or not. Cases where the bird is in the forward position and then does a short chase and immediately resumes the forward position, were marked as a single forward.
<b>Courtship</b>	<i>Full squat</i>	The bird has its body horizontal to the ground with head in line with the body and the bill points down. Ruff is spread. In the full squat the belly appears to contact the ground, in the half squat it does not. The bird performs the display alone.
	<i>Mutual squat</i>	The bird is in half squat or full squat posture, positioned in close proximity (near touching or touching) to another bird that is also in half squat or full squat posture. Both birds must be stationary, maintaining pose. The angle formed by the two birds' bodies (straight line from head to tail) was often around 90 degrees (perpendicular to one another), but birds could also be standing parallel to each other.
	<i>Circle</i>	Bird walks around another bird in a trajectory that traces one full round. This usually occurs before a mutual squat.
	<i>Half-circle</i>	Bird walks around another bird in a trajectory that completes a half-circle. This usually occurs before a mutual squat.
	<i>Mount</i>	Bird places its body on top of another bird and its belly makes contact to the back of the bird that is under it.
<b>Other</b>	<i>Bathing</i>	The bird stands inside the water bath actively rinsing its body with short partial or full immersion paired with head and body twisting
	<i>Flying</i>	The bird flies from a certain location of the enclosure to another.
	<i>Flapping</i>	The bird opens and moves its wings flapping them without flying.
	<i>Feeding</i>	The bird is eating or drinking.
	<i>Preening</i>	The bird is preening its feathers by running its beak along feather shafts.

**Table S5. Ethogram to quantify aggression and courtship behavior in male ruffs**

Ruff ethogram describing the 14 behaviors scored; aggression and courtship results are summarized in Fig. 1B. See Methods for details.

Gene symbol (this paper)	Gene symbol (NCBI)	NCBI Gene description	Genomic coordinates	Strand
<b>SLC7A5</b>	<i>LOC106888268</i>	large neutral amino acids transporter small subunit 1	NW_015090842.1: 8938536-8979141	minus
<b>SLC7A5</b>	<i>LOC106888122</i>	putative L-type amino acid transporter 1-like protein MLAS	NW_015090842.1: 8984146-8985026	minus
<b>TUBB3</b>	<i>LOC106888290</i>	tubulin beta chain-like	NW_015090842.1: 10204284-10206293	plus
<b>TUBB3</b>	<i>LOC106888291</i>	tubulin beta chain-like	NW_015090842.1: 10211366-10213320	plus
<b>CBFA2T3</b>	<i>LOC106888072</i>	protein CBFA2T3-like	NW_015090842.1: 9696891-9699541	minus
<b>CBFA2T3</b>	<i>LOC106888207</i>	protein CBFA2T3-like	NW_015090842.1: 9699619-9701252	minus
<b>CBFA2T3</b>	<i>LOC106888359</i>	protein CBFA2T3	NW_015090842.1: 9709383-9745127	minus
<b>ATP2C2</b>	<i>ATP2C2</i>	ATPase secretory pathway Ca <sup>2+</sup> transporting 2	NW_015090842.1: 7386778-7413905	plus
<b>ATP2C2</b>	<i>LOC106888386</i>	calcium-transporting ATPase type 2C member 2-like	NW_015090842.1: 7414345-7418829	plus
<b>TLDC1</b>	<i>MEAK7</i>	MTOR associated protein, eak-7 homolog	NW_015090842.1: 7421116-7432086	minus
<b>TLDC1</b>	<i>TLDC1</i>	MTOR associated protein, eak-7 homolog	NW_015090842.1: 7421116-7432086	minus
<b>COX4I1</b>	<i>LOC106888317</i>	cytochrome c oxidase subunit 4 isoform 1, mitochondrial	NW_015090842.1: 8439924-8443817	minus
<b>ARY2</b>	<i>LOC106888089</i>	arylamine N-acetyltransferase, pineal gland isozyme NAT-3	NW_015090842.1: 6296699-6307755	plus
<b>ARY1</b>	<i>LOC106888318</i>	arylamine N-acetyltransferase, liver isozyme-like	NW_015090842.1: 6310061-6313844	plus
<b>ARYL</b>	<i>LOC106888319</i>	arylamine N-acetyltransferase, pineal gland isozyme NAT-10	NW_015090842.1: 6313854-6319370	plus
<b>CYB5B</b>	<i>LOC106888329</i>	cytochrome b5	NW_015090842.1: 10336543-10349434	plus
<b>CYBA</b>	<i>LOC106888123</i>	cytochrome b-245 light chain	NW_015090842.1: 9547249-9548776	minus
<b>CDH3</b>	<i>LOC106888173</i>	B-cadherin-like	NW_015090842.1: 10239587-10243967	plus
<b>CDH1</b>	<i>LOC106888384</i>	cadherin-1-like	NW_015090842.1: 10244665-10255836	plus
<b>CDH1-like</b>	<i>LOC106888094</i>	cadherin-1-like	NW_015090842.1: 10233306-10236723	minus
<b>DUSP22A-like</b>	<i>LOC106888098</i>	dual specificity protein phosphatase 22-A-like	NW_015090842.1: 8422753-8437549	minus
<b>HNF4B</b>	<i>LOC106888312</i>	hepatocyte nuclear factor 4-beta-like	NW_015090842.1: 7705968-7733983	plus
<b>SULT2B1</b>	<i>LOC106888185</i>	sulfotransferase family cytosolic 2B member 1-like	NW_015090842.1: 10094914-10097611	minus

**Table S6. Reassigned gene symbol names located within inversion regions applied in this study**

List of genes for which we assigned gene names of putative homologs. We manually inspected gene structure of genes within the inversion and near the breakpoints and identified several genes that are listed as paralogs in the genome but are instead single genes and assigned the gene symbol listed here. Gene symbols in bold refer to genes that were merged and treated as a single gene in analyses. Genomic coordinates according to NCBI assembly GCF\_001431845.1.



Gene symbol	Gene description	Genomic coordinates	Strand
<i>AR</i>	androgen receptor	NW_015090995.1: 2974770-3034997	minus
<i>CENPN</i>	centromere protein N	NW_015090842.1: 5801588-5810753	plus
<i>DPEP1</i>	dipeptidase 1	NW_015090842.1: 10097985-10102081	plus
<i>ESR1</i>	estrogen receptor 1	NW_015090922.1: 36961838-37090930	plus
<i>ESR2</i>	estrogen receptor 2	NW_015090930.1: 930282-975805	minus
<i>FSHB</i>	follicle stimulating hormone subunit beta	NW_015090909.1: 615090-616065	plus
<i>GIN52</i>	GIN5 complex subunit 2	NW_015090842.1: 8466368-8471063	plus
<i>GPER1</i>	G protein-coupled estrogen receptor 1	NW_015090876.1: 2510905-2516625	minus
<i>HSD17B2</i>	hydroxysteroid 17-beta dehydrogenase 2	NW_015090842.1: 6257506-6268838	plus
<i>HSD17B3</i>	hydroxysteroid 17-beta dehydrogenase 3	NW_015090766.1: 2859822-2883752	minus
<i>LOC106889446 (CYP19A1)</i>	aromatase	NW_015090862.1: 7989778-8012648	minus
<i>LOC106894170 (GNRHR3)</i>	gonadotropin-releasing hormone receptor 3	NW_015090969.1: 2385180-2387552	minus
<i>LOC106896489 (GHI)</i>	growth hormone 1, somatotropin	NW_015091045.1: 2304329-2307869	plus
<i>LOC106896584 (CYP11A1)</i>	cholesterol side-chain cleavage enzyme, mitochondrial	NW_015091061.1: 468673-482272	minus
<i>LOC106896857 (HSD3B2)</i>	3-beta hydroxysteroid dehydrogenase/delta-5-delta-4 isomerase type 2	NW_015091072.1: 1268712-1278435	minus
<i>LOC106897604 (CYP17A1)</i>	steroid 17-alpha-hydroxylase/17,20 lyase	NW_015090781.1: 3575162-3580167	minus
<i>PGR</i>	progesterone receptor	NW_015094510.1: 31635551-31672696	plus
<i>PLCG2</i>	phospholipase C gamma 2	NW_015090842.1: 6179574-6231428	plus
<i>POMC</i>	proopiomelanocortin	NW_015090804.1: 199102-200571	minus
<i>PRL</i>	prolactin	NW_015090830.1: 23503863-23511518	minus
<i>SDR42E1</i>	short chain dehydrogenase/reductase family 42E, member 1	NW_015090842.1: 6235286-6238867	minus
<i>SRD5A1</i>	steroid 5-alpha reductase 1	NW_015090830.1: 1125837-1140656	plus
<i>SRD5A2</i>	steroid 5-alpha-reductase 2	NW_015090922.1: 20173392-20205430	plus
<i>STAR</i>	steroidogenic acute regulatory protein	NW_015091123.1: 1786403-1790949	minus
<i>TSHB</i>	thyroid stimulating hormone subunit beta	NW_015090898.1: 574405-576573	minus

**Table S7. Gene symbols and descriptions for main text and supplemental figures**

List of gene symbols, descriptions, genomic coordinates and strand information for genes that are shown as abbreviations in main and supplemental figures. Genomic coordinates according to NCBI assembly GCF\_001431845.1.

Plasmid name	GenBank accession	Description
pIRES2-AcGFP1-hHSD17B2-mycHis	PP539712	Expression vector for human HSD17B2
pIRES2-AcGFP1-IND_HSD17B2-mycHis	PP539713	Expression vector for ruff HSD17B2, independent allelic variant
pIRES2-AcGFP1-SAT_HSD17B2-mycHis	PP539714	Expression vector for ruff HSD17B2, satellite allelic variant
pIRES2-AcGFP1-FAE_HSD17B2-mycHis	PP539715	Expression vector for ruff HSD17B2, faeder allelic variant
pIRES2-AcGFP1-VAR1_HSD17B2-mycHis	PP539716	Expression vector for ruff HSD17B2, Var-1 synthetic variant
pIRES2-AcGFP1-VAR2_HSD17B2-mycHis	PP539717	Expression vector for ruff HSD17B2, Var-2 synthetic variant
pIRES2-AcGFP1-VAR3_HSD17B2-mycHis	PP539718	Expression vector for ruff HSD17B2, Var-3 synthetic variant
pIRES2-AcGFP1-VAR4_HSD17B2-mycHis	PP539719	Expression vector for ruff HSD17B2, Var-4 synthetic variant

**Table S8. Accession numbers for plasmids used in this study**

To examine the rate of testosterone conversion into androstenedione for ruff morph HSD17B2 isozymes and four synthetic HSD17B2 variants, we synthesized seven ruff-specific plasmids that express HSD17B2 in vitro. We created these constructs starting with the pIRES2-AcGFP1-hHSD17B2-mycHis plasmid (41). See Methods for cloning description and Fig. 3A for residue mutation details relative to independent HSD17B2.

## **Materials Design Analysis Reporting (MDAR)**

### **Checklist for Authors**

The MDAR framework establishes a minimum set of requirements in transparent reporting applicable to studies in the life sciences (see Statement of Task: [doi:10.31222/osf.io/9sm4x](https://doi.org/10.31222/osf.io/9sm4x)). The MDAR checklist is a tool for authors, editors, and others seeking to adopt the MDAR framework for transparent reporting in manuscripts and other outputs. Please refer to the MDAR Elaboration Document for additional context for the MDAR framework.

**For all that apply, please note where in the manuscript the required information is provided.**

**Materials:**

<b>Newly created materials</b>	<b>indicate where provided: page no/section/legend)</b>	<b>n/a</b>
The manuscript includes a dedicated "materials availability statement" providing transparent disclosure about availability of newly created materials including details on how materials can be accessed and describing any restrictions on access.	'Data and materials availability' section.	
<b>Antibodies</b>	<b>indicate where provided: page no/section/legend)</b>	<b>n/a</b>
For commercial reagents, provide supplier name, catalogue number and <a href="#">RRID</a> , if available.	Antibodies are listed throughout 'Materials and Methods' section.	
<b>DNA and RNA sequences</b>	<b>indicate where provided: page no/section/legend)</b>	<b>n/a</b>
<b>Short novel DNA or RNA including primers, probes:</b> Sequences should be included or deposited in a public repository.	RNA-Seq data is uploaded under BioProject PRJNA1099138 and plasmid sequences have been made publicly available, GenBank accession numbers are listed in table S8 of 'Materials and Methods'.	
<b>Cell materials</b>	<b>indicate where provided: page no/section/legend)</b>	<b>n/a</b>
<b>Cell lines:</b> Provide species information, strain. Provide accession number in repository <b>OR</b> supplier name, catalog number, clone number, <b>OR</b> RRID.	Transfections were carried out with HEK293 cells (Supplier ATCC) listed in 'Cell culture and transfection' subheading in 'Materials and Methods'.	
<b>Primary cultures:</b> Provide species, strain, sex of origin, genetic modification status.		<b>X</b>
<b>Experimental animals</b>	<b>indicate where provided: page no/section/legend)</b>	<b>n/a</b>
<b>Laboratory animals or Model organisms:</b> Provide species, strain, sex, age, genetic modification status. Provide accession number in repository <b>OR</b> supplier name, catalog number, clone number, <b>OR</b> RRID.	Listed in 'Materials and Methods' section under 'Animal breeding' subheading, captive bred flock.	
<b>Animal observed in or captured from the field:</b> Provide species, sex, and age where possible.		<b>X</b>
<b>Plants and microbes</b>	<b>indicate where provided: page no/section/legend)</b>	<b>n/a</b>
<b>Plants:</b> provide species and strain, ecotype and cultivar where relevant, unique accession number if available, and source (including location for collected wild specimens).		<b>X</b>
<b>Microbes:</b> provide species and strain, unique accession number if available, and source.		<b>X</b>
<b>Human research participants</b>	<b>indicate where provided: page no/section/legend) or state if these demographics were not collected</b>	<b>n/a</b>
If collected and within the bounds of privacy		<b>X</b>

constraints report on age, sex and gender or ethnicity for all study participants.		
--	--	--

## Design:

Study protocol	indicate where provided: page no/section/legend)	n/a
If study protocol has been pre-registered, provide DOI. For clinical trials, provide the trial registration number <b>OR</b> cite DOI.		X

Laboratory protocol	indicate where provided: page no/section/legend)	n/a
Provide DOI <b>OR</b> other citation details if detailed step-by-step protocols are available.		X

Experimental study design (statistics details)		
For in vivo studies: State whether and how the following have been done	indicate where provided: page no/section/legend. If it could have been done, but was not, write not done	n/a
Sample size determination		X
Randomisation		X
Blinding	Blinding applied in behavior scoring, described in 'Materials and Methods'	
Inclusion/exclusion criteria		X

Sample definition and in-laboratory replication	indicate where provided: page no/section/legend	n/a
State number of times the experiment was replicated in laboratory.	In 'Materials and Methods' section	
Define whether data describe technical or biological replicates.	In 'Materials and Methods' section	

Ethics	indicate where provided: page no/section/legend	n/a
<b>Studies involving human participants:</b> State details of authority granting ethics approval (IRB or equivalent committee(s), provide reference number for approval.		X
<b>Studies involving experimental animals:</b> State details of authority granting ethics approval (IRB or equivalent committee(s), provide reference number for approval.	Stated in 'Materials and Methods' section, 'Animal breeding' subheading: Animal Care Committee of Simon Fraser University (permit #1232B-17)	
<b>Studies involving specimen and field samples:</b> State if relevant permits obtained, provide details of authority approving study; if none were required, explain why.	All samples were collected from a captive population in Canada and were exported to Germany, using the following permits:  In 2017 Export BC-17-0036, Environment Canada Import 46f-G8787-2017/145-2, Bayerisches Staatministerium für Umwelt und Verbraucherschutz  In 2018 Export BC-18-0039, Environment Canada Import 46f-G8787-2018/179-2, Bayerisches	

	Staatministerium für Umwelt und Verbraucherschutz  In 2019 Export BC-2019-0013, Environment Canada Import 46f-G8787-2019/118-2, Bayerisches Staatministerium für Umwelt und Verbraucherschutz	
--	--	--

<b>Dual Use Research of Concern (DURC)</b>	<b>indicate where provided: page no/section/legend</b>	<b>n/a</b>
If study is subject to dual use research of concern regulations, state the authority granting approval and reference number for the regulatory approval.		<b>X</b>

## Analysis:

Attrition	indicate where provided: page no/section/legend	n/a
Describe whether exclusion criteria were preestablished. Report if sample or data points were omitted from analysis. If yes report if this was due to attrition or intentional exclusion and provide justification.	Low RNA-quality was an exclusion criteria and this is mentioned in the 'Materials and Methods' section.	
Statistics	indicate where provided: page no/section/legend	n/a
Describe statistical tests used and justify choice of tests.	Fisher's exact test, Kruskal-Wallis (when data did not follow a normal distribution), Two-tailed binomial test, Spearman correlation, Benjamini-Hochberg and Bonferroni corrections were applied for multiple testing. Statistical tests employed for RNA-Seq data analysis are described in 'Materials and Methods'. Sample sizes are stated in all Figure legends and table s4 summarizes RNA-Seq sample sizes.	
Data availability	indicate where provided: page no/section/legend	n/a
For newly created and reused datasets, the manuscript includes a data availability statement that provides details for access or notes restrictions on access.	All data used for analyses is publicly available. The manuscript includes a data availability statement on page 11.	
If newly created datasets are publicly available, provide accession number in repository <b>OR</b> DOI <b>OR</b> URL and licensing details where available.	RNA-Seq data accession code: BioProject PRJNA1099138 Plasmid accession codes: all available in GenBank, accession numbers listed in table S8 Genome accession code: RefSeq GCF_001431845.1 Additional datasets deposited at GitHub: <a href="https://github.com/azemella/Ruff_adults_RNASeq_gene_expression_2024">https://github.com/azemella/Ruff_adults_RNASeq_gene_expression_2024</a> Zenodo: <a href="https://doi.org/10.5281/zenodo.11032422">10.5281/zenodo.11032422</a>	
If reused data is publicly available provide accession number in repository <b>OR</b> DOI <b>OR</b> URL, <b>OR</b> citation.	Plasma testosterone and androstenedione were measured in <a href="https://doi.org/10.3389/fgene.2021.641620">https://doi.org/10.3389/fgene.2021.641620</a> and <a href="https://doi.org/10.1016/j.yhbeh.2020.104877">https://doi.org/10.1016/j.yhbeh.2020.104877</a>	
Code availability	indicate where provided: page no/section/legend	n/a
For all newly generated custom computer code/software/mathematical algorithm or re-used code essential for replicating the main findings of the study, the manuscript includes a data availability statement that provides details for access or notes restrictions.	All code used for data analysis and visualization is publicly available. The manuscript includes a code availability statement on page 11.	
If newly generated code is publicly available, provide accession number in repository, <b>OR</b> DOI <b>OR</b> URL and licensing details where available. State any restrictions on code availability or accessibility.	GitHub: <a href="https://github.com/azemella/Ruff_adults_RNASeq_gene_expression_2024">https://github.com/azemella/Ruff_adults_RNASeq_gene_expression_2024</a> Zenodo: <a href="https://doi.org/10.5281/zenodo.11032422">10.5281/zenodo.11032422</a>	
If reused code is publicly available provide accession number in repository <b>OR</b> DOI <b>OR</b> URL, <b>OR</b> citation.		<b>X</b>





## **Reporting**

MDAR framework recommends adoption of discipline-specific guidelines, established and endorsed through community initiatives. Journals have their own policy about requiring specific guidelines and recommendations to complement MDAR.

<b>Adherence to community standards</b>	<b>indicate where provided: page no/section/legend</b>	<b>n/a</b>
State if relevant guidelines (e.g., ICMJE, MIBBI, ARRIVE) have been followed, and whether a checklist (e.g., CONSORT, PRISMA, ARRIVE) is provided with the manuscript.	ARRIVE E10 guidelines were followed. No checklist provided.	

## References and Notes

1. R. F. Oliveira, Social modulation of androgens in vertebrates: Mechanisms and function. *Adv. Stud. Behav.* **34**, 165–239 (2004). [doi:10.1016/S0065-3454\(04\)34005-2](https://doi.org/10.1016/S0065-3454(04)34005-2)
2. M. Hau, Regulation of male traits by testosterone: Implications for the evolution of vertebrate life histories. *BioEssays* **29**, 133–144 (2007). [doi:10.1002/bies.20524](https://doi.org/10.1002/bies.20524) [Medline](#)
3. L. Fusani, Testosterone control of male courtship in birds. *Horm. Behav.* **54**, 227–233 (2008). [doi:10.1016/j.yhbeh.2008.04.004](https://doi.org/10.1016/j.yhbeh.2008.04.004) [Medline](#)
4. W. Goymann, J. C. Wingfield, Male-to-female testosterone ratios, dimorphism, and life history—What does it really tell us? *Behav. Ecol.* **25**, 685–699 (2014). [doi:10.1093/beheco/aru019](https://doi.org/10.1093/beheco/aru019)
5. D. J. Handelsman, A. L. Hirschberg, S. Berman, Circulating Testosterone as the Hormonal Basis of Sex Differences in Athletic Performance. *Endocr. Rev.* **39**, 803–829 (2018). [doi:10.1210/er.2018-00020](https://doi.org/10.1210/er.2018-00020) [Medline](#)
6. N. L. Staub, M. De Beer, The role of androgens in female vertebrates. *Gen. Comp. Endocrinol.* **108**, 1–24 (1997). [doi:10.1006/gcen.1997.6962](https://doi.org/10.1006/gcen.1997.6962) [Medline](#)
7. E. D. Ketterson, V. Nolan Jr., M. Sandell, Testosterone in females: Mediator of adaptive traits, constraint on sexual dimorphism, or both? *Am. Nat.* **166**, S85–S98 (2005). [doi:10.1086/444602](https://doi.org/10.1086/444602) [Medline](#)
8. N. Sinnott-Armstrong, S. Naqvi, M. Rivas, J. K. Pritchard, GWAS of three molecular traits highlights core genes and pathways alongside a highly polygenic background. *eLife* **10**, e58615 (2021). [doi:10.7554/eLife.58615](https://doi.org/10.7554/eLife.58615) [Medline](#)
9. W. Goymann, Social modulation of androgens in male birds. *Gen. Comp. Endocrinol.* **163**, 149–157 (2009). [doi:10.1016/j.ygcen.2008.11.027](https://doi.org/10.1016/j.ygcen.2008.11.027) [Medline](#)
10. M. Morkkonen, E. Koskela, T. Mappes, S. C. Mills, Sexual antagonism for testosterone maintains multiple mating behaviour. *J. Anim. Ecol.* **81**, 277–283 (2012). [doi:10.1111/j.1365-2656.2011.01903.x](https://doi.org/10.1111/j.1365-2656.2011.01903.x) [Medline](#)
11. R. F. Oliveira, M. Taborsky, H. J. Brockmann, Eds., *Alternative Reproductive Tactics: An Integrative Approach* (Cambridge Univ. Press, 2008).
12. J. E. Mank, Sex-specific morphs: The genetics and evolution of intra-sexual variation. *Nat. Rev. Genet.* **24**, 44–52 (2023). [doi:10.1038/s41576-022-00524-2](https://doi.org/10.1038/s41576-022-00524-2) [Medline](#)
13. A. T. Pavitt, C. A. Walling, J. M. Pemberton, L. E. B. Kruuk, Heritability and cross-sex genetic correlations of early-life circulating testosterone levels in a wild mammal. *Biol. Lett.* **10**, 20140685 (2014). [doi:10.1098/rsbl.2014.0685](https://doi.org/10.1098/rsbl.2014.0685) [Medline](#)
14. V. Bogaert, Y. Taes, P. Konings, K. Van Steen, D. De Bacquer, S. Goemaere, H. Zmierzak, P. Crabbe, J.-M. Kaufman, Heritability of blood concentrations of sex-steroids in relation to body composition in young adult male siblings. *Clin. Endocrinol. (Oxf.)* **69**, 129–135 (2008). [doi:10.1111/j.1365-2265.2008.03173.x](https://doi.org/10.1111/j.1365-2265.2008.03173.x) [Medline](#)
15. C. Ohlsson, H. Wallaschowski, K. L. Lunetta, L. Stolk, J. R. B. Perry, A. Koster, A.-K. Petersen, J. Eriksson, T. Lehtimäki, I. T. Huhtaniemi, G. L. Hammond, M. Maggio, A. D. Coviello, L. Ferrucci, M. Heier, A. Hofman, K. L. Holliday, J.-O. Jansson, M. Kähönen,

- D. Karasik, M. K. Karlsson, D. P. Kiel, Y. Liu, O. Ljunggren, M. Lorentzon, L.-P. Lyytikäinen, T. Meitinger, D. Mellström, D. Melzer, I. Miljkovic, M. Nauck, M. Nilsson, B. Penninx, S. R. Pye, R. S. Vasan, M. Reincke, F. Rivadeneira, A. Tajar, A. Teumer, A. G. Uitterlinden, J. Ulloor, J. Viikari, U. Völker, H. Völzke, H. E. Wichmann, T.-S. Wu, W. V. Zhuang, E. Ziv, F. C. W. Wu, O. Raitakari, A. Eriksson, M. Bidlingmaier, T. B. Harris, A. Murray, F. H. de Jong, J. M. Murabito, S. Bhasin, L. Vandenput, R. Haring; EMAS Study Group, Genetic determinants of serum testosterone concentrations in men. *PLOS Genet.* **7**, e1002313 (2011). [doi:10.1371/journal.pgen.1002313](https://doi.org/10.1371/journal.pgen.1002313) [Medline](#)
16. K. S. Ruth, F. R. Day, J. Tyrrell, D. J. Thompson, A. R. Wood, A. Mahajan, R. N. Beaumont, L. Wittemans, S. Martin, A. S. Busch, A. M. Erzurumluoglu, B. Hollis, T. A. O'Mara, M. I. McCarthy, C. Langenberg, D. F. Easton, N. J. Wareham, S. Burgess, A. Murray, K. K. Ong, T. M. Frayling, J. R. B. Perry; Endometrial Cancer Association Consortium, Using human genetics to understand the disease impacts of testosterone in men and women. *Nat. Med.* **26**, 252–258 (2020). [doi:10.1038/s41591-020-0751-5](https://doi.org/10.1038/s41591-020-0751-5) [Medline](#)
17. E. D. Ketterson, J. W. Atwell, J. W. McGlothlin, Phenotypic integration and independence: Hormones, performance, and response to environmental change. *Integr. Comp. Biol.* **49**, 365–379 (2009). [doi:10.1093/icb/icp057](https://doi.org/10.1093/icb/icp057) [Medline](#)
18. K. A. Rosvall, C. M. Bergeon Burns, S. P. Jayaratna, E. K. Dossey, E. D. Ketterson, Gonads and the evolution of hormonal phenotypes. *Integr. Comp. Biol.* **56**, 225–234 (2016). [doi:10.1093/icb/icw050](https://doi.org/10.1093/icb/icw050) [Medline](#)
19. K. K. Soma, N. M. Rendon, R. Boonstra, H. E. Albers, G. E. Demas, DHEA effects on brain and behavior: Insights from comparative studies of aggression. *J. Steroid Biochem. Mol. Biol.* **145**, 261–272 (2015). [doi:10.1016/j.jsbmb.2014.05.011](https://doi.org/10.1016/j.jsbmb.2014.05.011) [Medline](#)
20. C. Küpper, M. Stocks, J. E. Risse, N. Dos Remedios, L. L. Farrell, S. B. McRae, T. C. Morgan, N. Karlionova, P. Pinchuk, Y. I. Verkuil, A. S. Kitaysky, J. C. Wingfield, T. Piersma, K. Zeng, J. Slate, M. Blaxter, D. B. Lank, T. Burke, A supergene determines highly divergent male reproductive morphs in the ruff. *Nat. Genet.* **48**, 79–83 (2016). [doi:10.1038/ng.3443](https://doi.org/10.1038/ng.3443) [Medline](#)
21. A. J. Hogan-Warburg, Social behavior of the ruff *Philomachus pugnax* (L.). *Ardea* **54**, 109–229 (1966).
22. J. D. M. Tolliver, K. Kupán, D. B. Lank, S. Schindler, C. Küpper, Fitness benefits from co-display favour subdominant male–male partnerships between phenotypes. *Anim. Behav.* **197**, 131–154 (2023). [doi:10.1016/j.anbehav.2022.12.004](https://doi.org/10.1016/j.anbehav.2022.12.004)
23. J. Jukema, T. Piersma, Permanent female mimics in a lekking shorebird. *Biol. Lett.* **2**, 161–164 (2006). [doi:10.1098/rsbl.2005.0416](https://doi.org/10.1098/rsbl.2005.0416) [Medline](#)
24. J. L. Loveland, D. B. Lank, C. Küpper, Gene expression modification by an autosomal inversion associated with three male mating morphs. *Front. Genet.* **12**, 641620 (2021). [doi:10.3389/fgene.2021.641620](https://doi.org/10.3389/fgene.2021.641620) [Medline](#)
25. J. L. Loveland, L. M. Giraldo-Deck, D. B. Lank, W. Goymann, M. Gahr, C. Küpper, Functional differences in the hypothalamic-pituitary-gonadal axis are associated with alternative reproductive tactics based on an inversion polymorphism. *Horm. Behav.* **127**, 104877 (2021). [doi:10.1016/j.yhbeh.2020.104877](https://doi.org/10.1016/j.yhbeh.2020.104877) [Medline](#)

26. S. Lamichhaney, G. Fan, F. Widemo, U. Gunnarsson, D. S. Thalmann, M. P. Hoepfner, S. Kerje, U. Gustafson, C. Shi, H. Zhang, W. Chen, X. Liang, L. Huang, J. Wang, E. Liang, Q. Wu, S. M.-Y. Lee, X. Xu, J. Höglund, X. Liu, L. Andersson, Structural genomic changes underlie alternative reproductive strategies in the ruff (*Philomachus pugnax*). *Nat. Genet.* **48**, 84–88 (2016). [doi:10.1038/ng.3430](https://doi.org/10.1038/ng.3430) [Medline](#)
27. J. Hill, E. D. Enbody, H. Bi, S. Lamichhaney, W. Lei, J. Chen, C. Wei, Y. Liu, D. Schwochow, S. Younis, F. Widemo, L. Andersson, Low mutation load in a supergene underpinning alternative male mating strategies in ruff (*Calidris pugnax*). *Mol. Biol. Evol.* **40**, msad224 (2023). [doi:10.1093/molbev/msad224](https://doi.org/10.1093/molbev/msad224) [Medline](#)
28. J. L. Goodson, The vertebrate social behavior network: Evolutionary themes and variations. *Horm. Behav.* **48**, 11–22 (2005). [doi:10.1016/j.yhbeh.2005.02.003](https://doi.org/10.1016/j.yhbeh.2005.02.003) [Medline](#)
29. L. A. O’Connell, H. A. Hofmann, Evolution of a vertebrate social decision-making network. *Science* **336**, 1154–1157 (2012). [doi:10.1126/science.1218889](https://doi.org/10.1126/science.1218889) [Medline](#)
30. K. von Eugen, S. Tabrik, O. Güntürkün, F. Ströckens, A comparative analysis of the dopaminergic innervation of the executive caudal nidopallium in pigeon, chicken, zebra finch, and carrion crow. *J. Comp. Neurol.* **528**, 2929–2955 (2020). [doi:10.1002/cne.24878](https://doi.org/10.1002/cne.24878) [Medline](#)
31. M. Kapun, T. Flatt, The adaptive significance of chromosomal inversion polymorphisms in *Drosophila melanogaster*. *Mol. Ecol.* **28**, 1263–1282 (2019). [doi:10.1111/mec.14871](https://doi.org/10.1111/mec.14871) [Medline](#)
32. K. A. Rosvall, C. M. Bergeon Burns, S. P. Jayaratna, E. D. Ketterson, Divergence along the gonadal steroidogenic pathway: Implications for hormone-mediated phenotypic evolution. *Horm. Behav.* **84**, 1–8 (2016). [doi:10.1016/j.yhbeh.2016.05.015](https://doi.org/10.1016/j.yhbeh.2016.05.015) [Medline](#)
33. I. T. Huhtaniemi, I. T. Huhtaniemi; Themmen APN, Mutations of gonadotropins and gonadotropin receptors: Elucidating the physiology and pathophysiology of pituitary-gonadal function. *Endocr. Rev.* **21**, 551–583 (2000). [doi:10.1210/edrv.21.5.0409](https://doi.org/10.1210/edrv.21.5.0409) [Medline](#)
34. J. R. Merritt, K. E. Grogan, W. M. Zinzow-Kramer, D. Sun, E. A. Ortlund, S. V. Yi, D. L. Maney, A supergene-linked estrogen receptor drives alternative phenotypes in a polymorphic songbird. *Proc. Natl. Acad. Sci. U.S.A.* **117**, 21673–21680 (2020). [doi:10.1073/pnas.2011347117](https://doi.org/10.1073/pnas.2011347117) [Medline](#)
35. L. Wu, M. Einstein, W. M. Geissler, H. K. Chan, K. O. Elliston, S. Andersson, Expression cloning and characterization of human 17 beta-hydroxysteroid dehydrogenase type 2, a microsomal enzyme possessing 20 alpha-hydroxysteroid dehydrogenase activity. *J. Biol. Chem.* **268**, 12964–12969 (1993). [doi:10.1016/S0021-9258\(18\)31480-7](https://doi.org/10.1016/S0021-9258(18)31480-7) [Medline](#)
36. R. Mindnich, G. Möller, J. Adamski, The role of 17 beta-hydroxysteroid dehydrogenases. *Mol. Cell. Endocrinol.* **218**, 7–20 (2004). [doi:10.1016/j.mce.2003.12.006](https://doi.org/10.1016/j.mce.2003.12.006) [Medline](#)
37. C. Prehn, G. Möller, J. Adamski, Recent advances in 17beta-hydroxysteroid dehydrogenases. *J. Steroid Biochem. Mol. Biol.* **114**, 72–77 (2009). [doi:10.1016/j.jsbmb.2008.12.024](https://doi.org/10.1016/j.jsbmb.2008.12.024) [Medline](#)

38. J. L. Loveland, L. M. Giraldo-Deck, A. M. Kelly, How inversion variants can shape neural circuitry: Insights from the three-morph mating tactics of ruffs. *Front. Physiol.* **13**, 1011629 (2022). [doi:10.3389/fphys.2022.1011629](https://doi.org/10.3389/fphys.2022.1011629) [Medline](#)
39. E. L. Berdan, A. Blanckaert, R. K. Butlin, C. Bank, Deleterious mutation accumulation and the long-term fate of chromosomal inversions. *PLOS Genet.* **17**, e1009411 (2021). [doi:10.1371/journal.pgen.1009411](https://doi.org/10.1371/journal.pgen.1009411) [Medline](#)
40. M. Tsachaki, J. Birk, A. Egert, A. Odermatt, Determination of the topology of endoplasmic reticulum membrane proteins using redox-sensitive green-fluorescence protein fusions. *Biochim. Biophys. Acta* **1853**, 1672–1682 (2015). [doi:10.1016/j.bbamcr.2015.04.002](https://doi.org/10.1016/j.bbamcr.2015.04.002) [Medline](#)
41. C. P. Sager, S. Weber, M. Negri, P. Banachowicz, G. Möller, J. Adamski, R. W. Hartmann, S. Marchais-Oberwinkler, Homology modeling meets site-directed mutagenesis: An ideal combination to elucidate the topology of 17 $\beta$ -HSD2. *J. Steroid Biochem. Mol. Biol.* **206**, 105790 (2021). [doi:10.1016/j.jsbmb.2020.105790](https://doi.org/10.1016/j.jsbmb.2020.105790) [Medline](#)
42. L. Schiffer, A. Bossey, P. Kempegowda, A. E. Taylor, I. Akerman, D. Scheel-Toellner, K.-H. Storbeck, W. Arlt, Peripheral blood mononuclear cells preferentially activate 11-oxygenated androgens. *Eur. J. Endocrinol.* **184**, 353–363 (2021). [doi:10.1530/EJE-20-1077](https://doi.org/10.1530/EJE-20-1077) [Medline](#)
43. Z. Zhou, C. H. L. Shackleton, S. Pahwa, P. C. White, P. W. Speiser, Prominent sex steroid metabolism in human lymphocytes. *Mol. Cell. Endocrinol.* **138**, 61–69 (1998). [doi:10.1016/S0303-7207\(98\)00052-5](https://doi.org/10.1016/S0303-7207(98)00052-5) [Medline](#)
44. S. Andersson, N. Moghrabi, Physiology and molecular genetics of 17  $\beta$ -hydroxysteroid dehydrogenases. *Steroids* **62**, 143–147 (1997). [doi:10.1016/S0039-128X\(96\)00173-0](https://doi.org/10.1016/S0039-128X(96)00173-0) [Medline](#)
45. G. F. Ball, J. Balthazart, Hormonal regulation of brain circuits mediating male sexual behavior in birds. *Physiol. Behav.* **83**, 329–346 (2004). [doi:10.1016/j.physbeh.2004.08.020](https://doi.org/10.1016/j.physbeh.2004.08.020) [Medline](#)
46. L. Fusani, M. Gahr, J. B. Hutchison, Aromatase inhibition reduces specifically one display of the ring dove courtship behavior. *Gen. Comp. Endocrinol.* **122**, 23–30 (2001). [doi:10.1006/gcen.2001.7608](https://doi.org/10.1006/gcen.2001.7608) [Medline](#)
47. J. T. Watson, E. Adkins-Regan, Testosterone implanted in the preoptic area of male Japanese quail must be aromatized to activate copulation. *Horm. Behav.* **23**, 432–447 (1989). [doi:10.1016/0018-506X\(89\)90055-X](https://doi.org/10.1016/0018-506X(89)90055-X) [Medline](#)
48. T. Flatt, M.-P. Tu, M. Tatar, Hormonal pleiotropy and the juvenile hormone regulation of *Drosophila* development and life history. *BioEssays* **27**, 999–1010 (2005). [doi:10.1002/bies.20290](https://doi.org/10.1002/bies.20290) [Medline](#)
49. J. W. McGlothlin, E. D. Ketterson, in *Snowbird: Integrative Biology and Evolutionary Diversity in the Junco*, E. D. Ketterson, J. W. Atwell, Eds. (Univ. of Chicago Press, 2016), pp. 100–119.

50. T. N. Wittman, C. D. Robinson, J. W. McGlothlin, R. M. Cox, Hormonal pleiotropy structures genetic covariance. *Evol. Lett.* **5**, 397–407 (2021). [doi:10.1002/evl3.240](https://doi.org/10.1002/evl3.240) [Medline](#)
51. B. Dantzer, E. M. Swanson, Does hormonal pleiotropy shape the evolution of performance and life history traits? *Integr. Comp. Biol.* **57**, 372–384 (2017). [doi:10.1093/icb/ix064](https://doi.org/10.1093/icb/ix064) [Medline](#)
52. R. M. Cox, Sex steroids as mediators of phenotypic integration, genetic correlations, and evolutionary transitions. *Mol. Cell. Endocrinol.* **502**, 110668 (2020). [doi:10.1016/j.mce.2019.110668](https://doi.org/10.1016/j.mce.2019.110668) [Medline](#)
53. B. Gegenhuber, M. V. Wu, R. Bronstein, J. Tollkuhn, Gene regulation by gonadal hormone receptors underlies brain sex differences. *Nature* **606**, 153–159 (2022). [doi:10.1038/s41586-022-04686-1](https://doi.org/10.1038/s41586-022-04686-1) [Medline](#)
54. L. M. Giraldo-Deck, J. L. Loveland, W. Goymann, B. Tschirren, T. Burke, B. Kempnaers, D. B. Lank, C. Küpper, Intralocus conflicts associated with a supergene. *Nat. Commun.* **13**, 1384 (2022). [doi:10.1038/s41467-022-29033-w](https://doi.org/10.1038/s41467-022-29033-w) [Medline](#)
55. A. Zemella, *azemella/Ruff\_adults\_RNASeq\_gene\_expression\_2024: Update MD analysis and results, v6.0.0, Zenodo* (2024); <https://zenodo.org/records/14056330>.
56. D. B. Lank, L. L. Farrell, T. Burke, T. Piersma, S. B. McRae, A dominant allele controls development into female mimic male and diminutive female ruffs. *Biol. Lett.* **9**, 20130653 (2013). [doi:10.1098/rsbl.2013.0653](https://doi.org/10.1098/rsbl.2013.0653) [Medline](#)
57. D. B. Lank, M. Coupe, K. E. Wynne-Edwards, Testosterone-induced male traits in female ruffs (*Philomachus pugnax*): Autosomal inheritance and gender differentiation. *Proc. Biol. Sci.* **266**, 2323–2330 (1999). [doi:10.1098/rspb.1999.0926](https://doi.org/10.1098/rspb.1999.0926)
58. J. G. van Rhijn, Behavioural dimorphism in male ruffs, *Philomachus pugnax* (L.). *Behaviour* **47**, 153–227 (1973). [doi:10.1163/156853973X00076](https://doi.org/10.1163/156853973X00076)
59. L. Puelles, M. Martinez-de-la-Torre, S. Martinez, C. Watson, G. Paxinos, *The Chick Brain in Stereotaxic Coordinates and Alternate Stains: Featuring Neuromeric Divisions and Mammalian Homologies* (Academic Press, ed. 2, 2019).
60. W. J. Kuenzel, M. Masson, *A Stereotaxic Atlas of the Brain of the Chick (Gallus domesticus)* (Johns Hopkins University Press, 1988).
61. B. Cozzi, C. Viglietti-Panzica, N. Aste, G. C. Panzica, The serotonergic system in the brain of the Japanese quail. An immunohistochemical study. *Cell Tissue Res.* **263**, 271–284 (1991). [doi:10.1007/BF00318769](https://doi.org/10.1007/BF00318769) [Medline](#)
62. N. Aste, G. C. Panzica, C. Viglietti-Panzica, N. Harada, J. Balthazart, Distribution and effects of testosterone on aromatase mRNA in the quail forebrain: A non-radioactive in situ hybridization study. *J. Chem. Neuroanat.* **14**, 103–115 (1998). [doi:10.1016/S0891-0618\(97\)10023-0](https://doi.org/10.1016/S0891-0618(97)10023-0) [Medline](#)
63. S. Sen, P. Parishar, A. S. Pundir, A. Reiner, S. Iyengar, The expression of tyrosine hydroxylase and DARPP-32 in the house crow (*Corvus splendens*) brain. *J. Comp. Neurol.* **527**, 1801–1836 (2019). [doi:10.1002/cne.24649](https://doi.org/10.1002/cne.24649) [Medline](#)



64. A. Reiner, D. J. Perkel, L. L. Bruce, A. B. Butler, A. Csillag, W. Kuenzel, L. Medina, G. Paxinos, T. Shimizu, G. Striedter, M. Wild, G. F. Ball, S. Durand, O. Güntürkün, D. W. Lee, C. V. Mello, A. Powers, S. A. White, G. Hough, L. Kubikova, T. V. Smulders, K. Wada, J. Dugas-Ford, S. Husband, K. Yamamoto, J. Yu, C. Siang, E. D. Jarvis; Avian Brain Nomenclature Forum, Revised nomenclature for avian telencephalon and some related brainstem nuclei. *J. Comp. Neurol.* **473**, 377–414 (2004). [doi:10.1002/cne.20118](https://doi.org/10.1002/cne.20118) [Medline](#)
65. C. A. Paul, B. Beltz, J. Berger-Sweeney, The Nissl stain: a stain for cell bodies in brain sections. *Cold Spring Harb. Protoc.* **2008**, prot4805, (2008). [doi:10.1101/2023.09.27.559771v3](https://doi.org/10.1101/2023.09.27.559771v3) [Medline](#)
66. J. L. Loveland, N. Uy, K. P. Maruska, R. E. Carpenter, R. D. Fernald, Social status differences regulate the serotonergic system of a cichlid fish, *Astatotilapia burtoni*. *J. Exp. Biol.* **217**, 2680–2690 (2014). [doi:10.1242/jeb.100685](https://doi.org/10.1242/jeb.100685) [Medline](#)
67. W. J. Kuenzel, C. D. Golden, Distribution and change in number of gonadotropin-releasing hormone-1 neurons following activation of the photoneuroendocrine system in the chick, *Gallus gallus*. *Cell Tissue Res.* **325**, 501–512 (2006). [doi:10.1007/s00441-006-0191-7](https://doi.org/10.1007/s00441-006-0191-7) [Medline](#)
68. J. Balthazart, A. Foidart, C. Surlemont, N. Harada, Neuroanatomical specificity in the co-localization of aromatase and estrogen receptors. *J. Neurobiol.* **22**, 143–157 (1991). [doi:10.1002/neu.480220205](https://doi.org/10.1002/neu.480220205) [Medline](#)
69. J. M. Wild, J. Balthazart, Neural pathways mediating control of reproductive behavior in male Japanese quail. *J. Comp. Neurol.* **521**, 2067–2087 (2013). [doi:10.1002/cne.23275](https://doi.org/10.1002/cne.23275) [Medline](#)
70. E. Adkins-Regan, J. T. Watson, Sexual dimorphism in the avian brain is not limited to the song system of songbirds: A morphometric analysis of the brain of the quail (*Coturnix japonica*). *Brain Res.* **514**, 320–326 (1990). [doi:10.1016/0006-8993\(90\)91427-I](https://doi.org/10.1016/0006-8993(90)91427-I) [Medline](#)
71. L. A. O’Connell, H. A. Hofmann, The vertebrate mesolimbic reward system and social behavior network: A comparative synthesis. *J. Comp. Neurol.* **519**, 3599–3639 (2011). [doi:10.1002/cne.22735](https://doi.org/10.1002/cne.22735) [Medline](#)
72. T. Fujita, N. Aoki, C. Mori, K. J. Homma, S. Yamaguchi, Molecular biology of serotonergic systems in avian brains. *Front. Mol. Neurosci.* **16**, 1226645 (2023). [doi:10.3389/fnmol.2023.1226645](https://doi.org/10.3389/fnmol.2023.1226645) [Medline](#)
73. K. Yamamoto, P. Vernier, The evolution of dopamine systems in chordates. *Front. Neuroanat.* **5**, 21 (2011). [doi:10.3389/fnana.2011.00021](https://doi.org/10.3389/fnana.2011.00021) [Medline](#)
74. C. V. Mello, T. Kaser, A. A. Buckner, M. Wirthlin, P. V. Lovell, Molecular architecture of the zebra finch arcopallium. *J. Comp. Neurol.* **527**, 2512–2556 (2019). [doi:10.1002/cne.24688](https://doi.org/10.1002/cne.24688) [Medline](#)
75. C. H. Leung, D. F. Abebe, S. E. Earp, C. T. Goode, A. V. Grozhik, P. Mididoddi, D. L. Maney, Neural distribution of vasotocin receptor mRNA in two species of songbird. *Endocrinology* **152**, 4865–4881 (2011). [doi:10.1210/en.2011-1394](https://doi.org/10.1210/en.2011-1394) [Medline](#)



76. A. Dobin, C. A. Davis, F. Schlesinger, J. Drenkow, C. Zaleski, S. Jha, P. Batut, M. Chaisson, T. R. Gingeras, STAR: Ultrafast universal RNA-seq aligner. *Bioinformatics* **29**, 15–21 (2013). [doi:10.1093/bioinformatics/bts635](https://doi.org/10.1093/bioinformatics/bts635) [Medline](#)
77. G. A. Van der Auwera, B. D. O'Connor, *Genomics in the cloud: Using Docker, GATK, and WDL in Terra* (O'Reilly Media, 2020).
78. P. Danecek, J. K. Bonfield, J. Liddle, J. Marshall, V. Ohan, M. O. Pollard, A. Whitwham, T. Keane, S. A. McCarthy, R. M. Davies, H. Li, Twelve years of SAMtools and BCFtools. *Gigascience* **10**, giab008 (2021). [doi:10.1093/gigascience/giab008](https://doi.org/10.1093/gigascience/giab008) [Medline](#)
79. W. McLaren, L. Gil, S. E. Hunt, H. S. Riat, G. R. S. Ritchie, A. Thormann, P. Flicek, F. Cunningham, The Ensembl variant effect predictor. *Genome Biol.* **17**, 122 (2016). [doi:10.1186/s13059-016-0974-4](https://doi.org/10.1186/s13059-016-0974-4) [Medline](#)
80. B. Kaminow, S. Ballouz, J. Gillis, A. Dobin, Pan-human consensus genome significantly improves the accuracy of RNA-seq analyses. *Genome Res.* **32**, 738–749 (2022). [doi:10.1101/gr.275613.121](https://doi.org/10.1101/gr.275613.121) [Medline](#)
- 81 S. E. Castel, A. Levy-Moonshine, P. Mohammadi, E. Banks, T. Lappalainen, Tools and best practices for data processing in allelic expression analysis. *Genome Biol.* **16**, 195 (2015). [doi:10.1186/s13059-015-0762-6](https://doi.org/10.1186/s13059-015-0762-6) [Medline](#)
82. M. I. Love, W. Huber, S. Anders, Moderated estimation of fold change and dispersion for RNA-seq data with DESeq2. *Genome Biol.* **15**, 550 (2014). [doi:10.1186/s13059-014-0550-8](https://doi.org/10.1186/s13059-014-0550-8) [Medline](#)
83. J. Huerta-Cepas, D. Szklarczyk, D. Heller, A. Hernández-Plaza, S. K. Forslund, H. Cook, D. R. Mende, I. Letunic, T. Rattei, L. J. Jensen, C. von Mering, P. Bork, eggNOG 5.0: A hierarchical, functionally and phylogenetically annotated orthology resource based on 5090 organisms and 2502 viruses. *Nucleic Acids Res.* **47**, D309–D314 (2019). [doi:10.1093/nar/gky1085](https://doi.org/10.1093/nar/gky1085) [Medline](#)
84. M. Carlson, H. Pagès, AnnotationForge: Tools for building SQLite-based annotation data packages, R package version 1.44.0 (2023); <https://doi.org/10.18129/B9.bioc.AnnotationForge>
85. T. Wu, E. Hu, S. Xu, M. Chen, P. Guo, Z. Dai, T. Feng, L. Zhou, W. Tang, L. Zhan, X. Fu, S. Liu, X. Bo, G. Yu, clusterProfiler 4.0: A universal enrichment tool for interpreting omics data. *Innovation* **2**, 100141 (2021). [Medline](#)
86. W. Goymann, M. L. East, H. Hofer, Androgens and the role of female “hyperaggressiveness” in spotted hyenas (*Crocuta crocuta*). *Horm. Behav.* **39**, 83–92 (2001). [doi:10.1006/hbeh.2000.1634](https://doi.org/10.1006/hbeh.2000.1634) [Medline](#)
87. J. Jumper, R. Evans, A. Pritzel, T. Green, M. Figurnov, O. Ronneberger, K. Tunyasuvunakool, R. Bates, A. Židek, A. Potapenko, A. Bridgland, C. Meyer, S. A. A. Kohli, A. J. Ballard, A. Cowie, B. Romera-Paredes, S. Nikolov, R. Jain, J. Adler, T. Back, S. Petersen, D. Reiman, E. Clancy, M. Zielinski, M. Steinegger, M. Pacholska, T. Berghammer, S. Bodenstein, D. Silver, O. Vinyals, A. W. Senior, K. Kavukcuoglu, P. Kohli, D. Hassabis, Highly accurate protein structure prediction with AlphaFold. *Nature* **596**, 583–589 (2021). [doi:10.1038/s41586-021-03819-2](https://doi.org/10.1038/s41586-021-03819-2) [Medline](#)

88. J. P. G. L. M. Rodrigues, J. M. C. Teixeira, M. Trellet, A. M. J. J. Bonvin, pdb-tools: A swiss army knife for molecular structures. *F1000 Res.* **7**, 1961 (2018). [doi:10.12688/f1000research.17456.1](https://doi.org/10.12688/f1000research.17456.1) [Medline](#)
89. C. Dominguez, R. Boelens, A. M. J. J. Bonvin, HADDOCK: A protein-protein docking approach based on biochemical or biophysical information. *J. Am. Chem. Soc.* **125**, 1731–1737 (2003). [doi:10.1021/ja026939x](https://doi.org/10.1021/ja026939x) [Medline](#)
90. G. C. P. van Zundert, J. P. G. L. M. Rodrigues, M. Trellet, C. Schmitz, P. L. Kastitis, E. Karaca, A. S. J. Melquiond, M. van Dijk, S. J. de Vries, A. M. J. J. Bonvin, The HADDOCK2.2 web server: User-friendly integrative modeling of biomolecular complexes. *J. Mol. Biol.* **428**, 720–725 (2016). [doi:10.1016/j.jmb.2015.09.014](https://doi.org/10.1016/j.jmb.2015.09.014) [Medline](#)
91. Z. Kurcuoglu, P. I. Koukos, N. Citro, M. E. Trellet, J. P. G. L. M. Rodrigues, I. S. Moreira, J. Roel-Touris, A. S. J. Melquiond, C. Geng, J. Schaarschmidt, L. C. Xue, A. Vangone, A. M. J. J. Bonvin, Performance of HADDOCK and a simple contact-based protein-ligand binding affinity predictor in the D3R Grand Challenge 2. *J. Comput. Aided Mol. Des.* **32**, 175–185 (2018). [doi:10.1007/s10822-017-0049-y](https://doi.org/10.1007/s10822-017-0049-y) [Medline](#)
92. A. Vangone, J. Schaarschmidt, P. Koukos, C. Geng, N. Citro, M. E. Trellet, L. C. Xue, A. M. J. J. Bonvin, Large-scale prediction of binding affinity in protein-small ligand complexes: The PRODIGY-LIG web server. *Bioinformatics* **35**, 1585–1587 (2019). [doi:10.1093/bioinformatics/bty816](https://doi.org/10.1093/bioinformatics/bty816) [Medline](#)
93. Z. Yang, PAML 4: Phylogenetic analysis by maximum likelihood. *Mol. Biol. Evol.* **24**, 1586–1591 (2007). [doi:10.1093/molbev/msm088](https://doi.org/10.1093/molbev/msm088) [Medline](#)
94. S. Álvarez-Carretero, P. Kapli, Z. Yang, Beginner’s guide on the use of PAML to detect positive selection. *Mol. Biol. Evol.* **40**, msad041 (2023). [doi:10.1093/molbev/msad041](https://doi.org/10.1093/molbev/msad041) [Medline](#)
95. B. Q. Minh, H. A. Schmidt, O. Chernomor, D. Schrempf, M. D. Woodhams, A. von Haeseler, R. Lanfear, IQ-TREE 2: New models and efficient methods for phylogenetic inference in the genomic era. *Mol. Biol. Evol.* **37**, 1530–1534 (2020). [doi:10.1093/molbev/msaa015](https://doi.org/10.1093/molbev/msaa015) [Medline](#)
96. F. Mölder, K. P. Jablonski, B. Letcher, M. B. Hall, C. H. Tomkins-Tinch, V. Sochat, J. Forster, S. Lee, S. O. Twardziok, A. Kanitz, A. Wilm, M. Holtgrewe, S. Rahmann, S. Nahnsen, J. Köster, Sustainable data analysis with Snakemake. *F1000 Res.* **10**, 33 (2021). [doi:10.12688/f1000research.29032.2](https://doi.org/10.12688/f1000research.29032.2) [Medline](#)
97. E. M. Wenzel, L. A. Elfmark, H. Stenmark, C. Raiborg, ER as master regulator of membrane trafficking and organelle function. *J. Cell Biol.* **221**, e202205135 (2022). [doi:10.1083/jcb.202205135](https://doi.org/10.1083/jcb.202205135) [Medline](#)